Tellus (2000), 52B, 141–168
Printed in UK. All rights reserved

TELLUS
ISSN 0280–6509

Chemical mass closure and assessment of the origin of the submicron aerosol in the marine boundary layer and the free troposphere at Tenerife during ACE-2

By J.-P. PUTAUD[1]*, R. VAN DINGENEN[1], M. MANGONI[1], A. VIRKKULA[1]**, F. RAES[1], H. MARING[2], J. M. PROSPERO[2], E. SWIETLICKI[3], O. H. BERG[3], R. HILLAMO[4] and T. MÄKELÄ[4], [1]*European Commission, Joint Research Centre, Environment Institute, TP 460, I-21020 Ispra (Va), Italy;* [2]*Institute for Marine and Atmospheric Studies, RSMAS, University of Miami, 4600 Rickenbacker Causeway, Miami, Florida 33149-1098, USA;* [3]*Division of Nuclear Physics, Lund University, Box 118, S-221 00 Lund, Sweden;* [4]*Finnish Meteorological Institute, Air Quality Research, Sahaajankatu 20E, FIN-00810 Helsinki, Finland*

(Manuscript received 1 March 1999; in final form 13 September 1999)

ABSTRACT

The organic, inorganic, mineral content and mass concentration of the submicron aerosol were measured in June–July 1997 on Tenerife in the marine boundary layer (MBL) and the free troposphere (FT). Aerosol size distributions were measured simultaneously at the same sites. The submicron aerosol mass concentrations derived from the chemical composition and calculated from the number size distributions agreed within the experimental uncertainties both in the MBL (±47%) and the FT (±75%). However, the analytical uncertainties in the concentration of organic compounds (OC) for the average sample collected in the MBL (−97, +77%) and the FT (±74%) were high. The average contribution of aerosol various components to the submicron aerosol mass were calculated for different air masses. The absolute uncertainties in these contributions were calculated by adding random uncertainties quadratically and possibly systematic errors in a conservative way. In the unperturbed MBL, the aerosol average composition (± the absolute uncertainty in the contribution) was 37 (−3, +9)% for non-sea-salt $SO_4^{2-} + NH_4^+$, 21 (−2, +10)% for sea-salt, and 20 (−7, +11)% OC ($N = 19$). In the unperturbed FT, OC and SO_4^{2-} accounted for 43 (±20)% and 32 (−5, +3)% of the submicron aerosol mass, respectively ($N = 15$). Considering these aerosol compositions, we suggest that the source for the FT aerosol could be the transport of continental aerosol through precipitating convective clouds. A simple budget calculation shows, that in background conditions, the MBL and FT aerosol compositions are consistent with the hypothesis that the MBL aerosol is formed by the dilution of continental aerosol by FT air, modified by deposition and condensation of species of oceanic origin. Dramatic continental aerosol outbreaks were observed in both the MBL and the FT. The aerosol outbreaks in the MBL were due to transport of polluted air masses from Europe. They were characterized mainly by increases in $SO_4^{2-} + NH_4^+$, making up 75 (−5, +19)% of the submicron aerosol mass. The aerosol outbreaks in the FT were due to advection of desert dust, probably mixed with pollution aerosol.

* Corresponding author.
e-mail: jean.putaud@jrc.it
** Present affiliation: Finnish Meteorological Institute, Helsinki, Finland.

1. Introduction

The direct and indirect effects of aerosols on the radiative balance of the Earth are still very uncertain (IPCC, 1996). Reducing the uncertainties in aerosol forcing needs a better representation of the aerosol in global models. However, the number and complexity of the processes determining the radiative properties and the cloud condensation nucleus (CCN) formation potential of an aerosol population are such that the aerosol system is not easily treated explicitly in global models. Based on emission inventories, global models typically calculate mass concentration fields of chemical species. One of the goals of the IGAC Aerosol Characterisation Experiments (ACE) is to establish accurate relationships linking aerosol mass concentrations and radiative and cloud nucleating properties. This can be achieved by formulating empirical relationships between these parameters. However, a higher confidence level is reached when an aerosol property calculated from theoretical laws and the aerosol chemical characteristics can be compared successfully with a direct measurement of this aerosol property. A basic requirement in any such calculation is the complete and accurate determination of the aerosol chemical composition.

This work presents the submicron aerosol chemical characterization at two ACE-2 ground sites on Tenerife: the lighthouse of Punta del Hidalgo (PDH), 55 m a.s.l. and the Izaña Observatory (IZO), 2370 m a.s.l. We first investigate how well the submicron aerosol at both sites can be described as a mixture of the measured organic, inorganic and mineral dust components. To do this, we compare three independent estimates of the submicron aerosol mass concentration m_{GM}, m_{CA}, and m_{SD}, calculated from gravimetric measurements (GM), from chemical analyses (CA) and from particle number size distribution measurements (SD), respectively. The uncertainties associated with each of the methods are analysed rigorously, and the differences between these three independent estimates compared to these uncertainties.

From this mass closure experiment, we determine the uncertainties in the submicron aerosol chemical composition observed in various synoptic situations. In the second part of the paper, we use the aerosol composition and associated uncertainties to investigate the possible origins of the free troposphere (FT) and marine boundary layer (MBL) aerosol in background conditions, as well as the sources of the aerosol outbreaks.

2. Experimental set-up

2.1. Sites and meteorology

The measurements were made between 17 June 1997 and 27 July 1997 on Tenerife Island (28°18′N, 16°30′W, Fig. 1) at PDH and IZO. PDH is located at sea-level at the North tip of the island. The measurements were performed from the top of a 50m high lighthouse to limit the influence of local sources (traffic, sea-spray produced by the waves breaking on the rocky shore). The Izaña observatory (IZO) is located at 2370 m a.s.l., at the end of a private road, on a volcanic peak where the vegetation is sparse. IZO is a Global Atmospheric Watch station, run by the Instituto Nacional de Meteorologia (INM). In summer, IZO is located well above the upper boundary of the MBL (1500 m). Trace gas measurements show that during night-time the site is representative of the FT (Fischer et al., 1998). During day-time, surface thermal winds cause upslope flow to IZO possibly bringing polluted low altitude air (Raes et al., 1997).

Fig. 1 shows that during ACE-2 air masses coming from (a) Europe, (b) Arctic and (c) Atlantic oceanic regions arrived at PDH, while at IZO, we sampled air masses of (a) African, (b) Arctic, (c) Atlantic and (d) North American origin. The parameters controlling the MBL and FT flows are discussed by Verver et al. (2000).

2.2. Aerosol sampling and analysis

2.2.1. Sampling. The sampling set-up at PDH is described in Fig. 2a. Aerosol was collected through PM10 inlets situated 2 m above the lighthouse top platform (55 m a.s.l.). Sampling was controlled to avoid local contamination according to wind speed, wind direction and CN count variations. Aerosol particles were collected at ambient relative humidity ($72 \pm 5\%$) over 12-h periods (08:00–20:00, and 20:00–08:00 UTC) using 2 virtual impactors (VI) built at the Finnish Meteorological Institute (FMI) based on Loo and Cork's (1988) design. At the flow rate of 18.3 L/min used during this experiment, the VI's

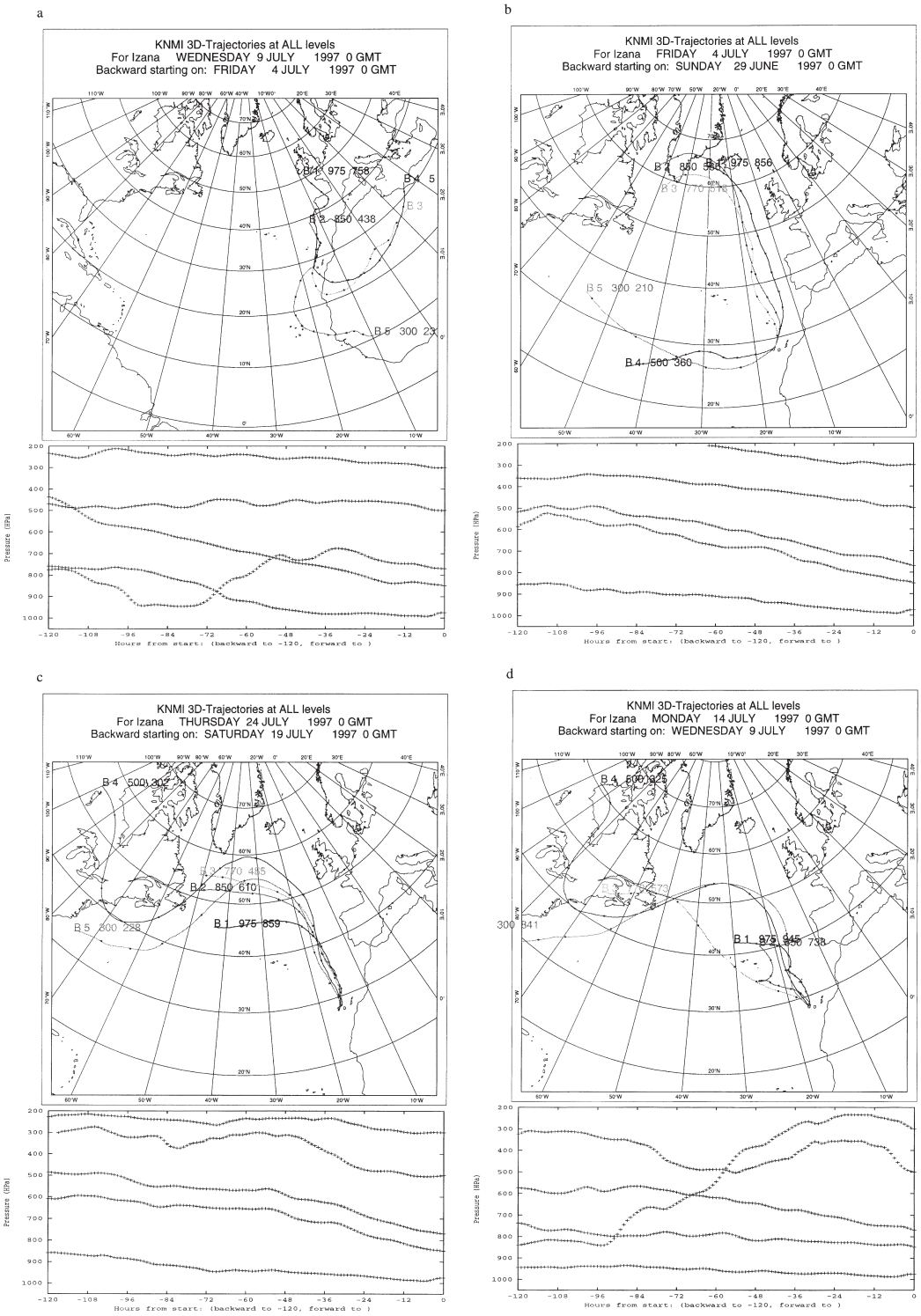

Fig. 1. Examples of 5 day back trajectories showing (a) transport of air masses from Europe and Africa in the MBL and the FT, respectively, (b) Arctic and (c) Atlantic flows in both the MBL and the FT, and (d) convection above America.

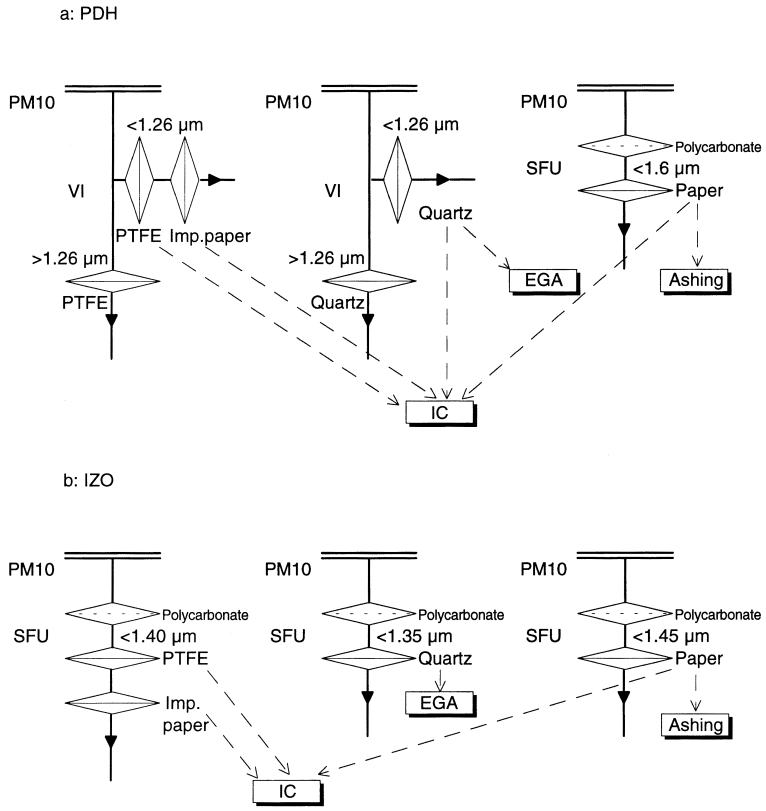

Fig. 2. Sampling principle and analytical methods used for (a) PDH and (b) IZO.

50% cut-off is 1.26 ± 0.05 µm aerodynamic diameter, with an impaction efficiency as a function of the particle diameter which was used for further calculations. One VI sampled on 1 µm pore size PTFE membranes (Millipore, FALP04700) and the other one on quartz fiber filters (PALLFLEX 2500QAT-UP) pre-fired at 800°C. PTFE membranes were chosen for gravimetric plus ion chromatography (IC) analyses and quartz filters for carbonaceous species analyses. During ACE-2, systematic differences were observed in the analysis of the samples from these two VIs (e.g., 19% for $nssSO_4$ and 41% Na^+, Fig. 9). They were attributed to slightly different sampling efficiencies in the two VIs. Carbonate-impregnated Whatman 41 filters were placed downstream of the PTFE fine fraction filter to correct potential losses of semi-volatile species from the PTFE membranes. A NILU 2–stacked filter unit (SFU) was used for determining mineral dust concentrations. With 8 µm pore size Apiezon coated polycarbonate membranes (Nuclepore) as initial filters, the SFU 50% cut-off was 1.6 ± 0.1 µm aerodynamic diameter at the face velocity of 27 cm s^{-1} (John et al., 1983). The Whatman 41 filters placed in the SFU second stage were washed $3\times$ in 18.2 MΩ cm resistivity water (mQ™) before use. The comparison of the Na^+ concentrations measured from the SFU and from the VIs during ACE-2 showed that the SFU collected $2\times$ more sea salt than the VI, due to its bigger cut-off diameter. As mineral dust is expected to be concentrated in supermicron particles, like sea-salt, this suggests that submicron mineral dust concentrations could be overestimated by up to 100%.

Assuming a dry aerosol density of 1.7 ± 0.2, and based on an aerosol growth factor (1.38 ± 0.1) at ambient relative humidity ($72 \pm 5\%$) derived from measurements performed at PDH (Swietlicki et al., 2000), we calculated an average ambient aerosol

density of 1.27 g cm^{-3} which leads to an equivalent dry (20% RH) cut-off of 0.85 ± 0.09 μm (geometric diameter) for the VIs and 1.08 ± 0.12 μm for the SFU. The cut-off calculation principle and the associated uncertainties are presented in Section 9 (Table 11).

The sampling set-up at IZO is described in Fig. 2b. Aerosol was collected through PM10 inlets located 2m above the flat platform of the IZO tower which is situated 15m above the ground. Samples were collected during night-time only (20:00–8:00 UTC). Three identical SFUs collected aerosol samples using an 8 μm pore size polycarbonate Apiezon coated filter (Nuclepore) in the first stage and PTFE, quartz fiber and washed Whatman 41 filters in the second stage for specific analyses of mass and ions, carbonaceous species, and mineral dust, respectively. The SFUs' 50% cut-offs were 1.35–1.45 μm aerodynamic diameter, according to the face velocity measured in each (John et al., 1983). Carbonate-impregnated Whatman 41 were placed downstream of the PTFE filter to assess possible losses. The ionic species concentrations measured from two of the three SFU samplers were compared. The systematic differences ranged from 6% for SO_4^{2-} to 36% for Ca^{2+} (Fig. 10), and were attributed to small differences in the SFUs' cut-off diameters.

Assuming a dry aerosol density of 1.7 ± 0.2 and an aerosol growth factor of 1.05 (-0.05, $+0.15$) at ambient relative humidity (20 ± 20%), we calculated an average particle density of 1.60 g cm^{-3} which leads to an equivalent dry (0% RH) cut-off of 1.05 (-0.11, $+0.20$) μm (geometric diameter) for the three SFUs. The cut-off calculation principle and the associated uncertainties are presented in Section 9 (Table 11).

Although the aerosol samplers' 50% cut-off diameters were not rigorously equal to 1.0 μm, we refer to the aerosol fine fraction collected during this experiment as submicron aerosol throughout this work.

2.2.2. Analyses and data processing. The PTFE filters used for IC analyses were also used for gravimetric measurements. They were weighed at JRC with a microbalance (Sartorius, MC5) at 23 ± 1°C and 19 ± 3% RH before and after sample collection. The balance was placed in a glove box made of Plexiglas coated with an anti-static spray to limit electrostatic effects. The filters were exposed for about 20 s to a radioactive ^{210}Po source to remove electrostatic charges. The glove box was continuously flushed with dried compressed air which passed through a cartridge of citric acid, potassium carbonate and activated charcoal. The air circulated over a temperature controlled water bath to obtain a constant RH in the glove box. The weighing precision was ± 1 μg. The microbalance was automatically calibrated every 5th sample. The standard variation of the PTFE blank filters was ± 3.4 and ± 8.7 μg for the series handled at PDH and IZO, respectively.

Including the (1) weighing precision, (2) the blank variability and (3) the uncertainty in the sampled air volume, the overall uncertainty of the aerosol mass concentration m_{GM} for the average sample was -10, $+12$% and ± 76% for PDH and IZO samples, respectively (Table 8). In several samples, the mass measured after sampling was lower than before sampling. This was attributed to inadequately prevented electrostatic effects and these samples were disregarded.

For mineral dust quantification, Whatman 41 filters were ashed at 600°C for 8 hours in quartz crucibles after extraction of water soluble species in mQ™ water. The residue was considered to be mineral dust, and was weighed using a microbalance (Sartorius, MC5) at 23°C and 19% RH. The blank levels were high (13 ± 4 μg/filter) and the mean residue obtained from samples (15 ± 6 μg) was not significantly higher than the mean residue obtained from blanks. This shows that most samples did not contain a detectable amount of mineral dust. The variability of the blanks introduced a very high uncertainty in mineral dust content quantification. Including the uncertainties assessed from the sampler intercomparison, the overall uncertainty in mineral dust concentration reaches -350, $+250$% and -390, $+350$% at PDH and IZO, respectively. The measured mass of dust was not corrected for possible losses of H_2O from hydrates during ashing, due to the lack of information regarding the origin and mineral composition of this dust.

PTFE filters were analysed by ion chromatography for Na^+, NH_4^+, K^+, Mg^{2+}, Ca^{2+}, acetate, formate, methanesulfonate (MSA), pyruvate, Cl^-, NO_3^-, SO_4^{2-} and oxalate. An intercomparison performed among the ACE-2 participants before the campaign showed that the uncertainty of the

IC analyses was $\pm 10\%$ for all species except Ca^{2+} (Section 6). IC analyses were also performed on all other filters except the Quartz filters sampled at IZO. The lowest blank values were observed on PTFE filters. The PTFE filter data are therefore used in the rest of the paper. IC data from the other filter types were used to assess the consistency of the samplers. The mean blank to sample ratio was 4% for NO_3^-, about 20% for the major species (Na^+, NH_4^+, MSA, and SO_4^{2-}), and up to 60% for Ca^{2+}. The blank variability generated uncertainties in the concentrations of the species analysed by IC of 3 to 9% and 5 to 42% at PDH and IZO, respectively.

The organic acids analysed by IC were gathered in a group named OA (OA = acetate + formate + MSA + pyruvate + oxalate). At PDH, the aerosol Na^+/Mg^{2+} ratio was equal to its sea water ratio, which suggests that sea spray was the main source for both. Non-sea-salt fractions (e.g., $nssSO_4^{2-}$) were calculated using Na^+ as a sea-salt tracer and a standard sea salt composition. Non-sea-salt K^+ and Ca^{2+} were added to the mineral ash into the group called "dust". Sea salt was calculated from the Na^+ concentrations, the ratio of K^+, Mg^{2+}, Ca^{2+} and SO_4^{2-} over Na^+ in standard sea water and the measured Cl^- concentrations to account for possible Cl^- depletion. NO_3^- was corrected for losses from PTFE filters assuming that all NO_3^- found in the carbonate-impregnated Whatman filter was due to the volatilization of particulate NO_3^- initially trapped on the submicron PTFE filter. The correction averaged 40% of the reported NO_3^- values, which is taken into account in the uncertainty analysis (Table 9).

At IZO, the regressions between Na^+, K^+, Mg^{2+}, Ca^{2+} and Cl^- did not indicate sea spray to be a major source for these species. Therefore, they were combined in a category called "salts". Since there was no evidence of sea salt in the submicron aerosol at IZO, we have assumed all measured SO_4^{2-} to be $nssSO_4^{2-}$. Unlike the MBL, the NO_3^- concentration found in the carbonate-impregnated Whatman was on average $25\times$ higher than that found on the up-stream PTFE filter. This ratio dropped to about 1 during dust conditions. According to measurements made from the Citation aircraft during ACE-2 (Joachim Curtius, personal communication, 1999), the concentration of gaseous nitric acid observed in the FT was sufficient to account for the amount of NO_3^- found in the carbonate impregnated Whatman filter. Therefore, we did not consider this NO_3^- fraction to be part of particulate NO_3^-. This choice was taken into account in the uncertainty analysis.

Including (1) the accuracy of IC analyses, (2) the blank variability, (3) the correction of possible sampling artifacts, (4) the comparison between samplers, and (5) the uncertainty in the sampled air volume, the uncertainty in the sum of the IC-analysed species concentrations is -8, $+9\%$ and -12, $+150\%$ at PDH and IZO, respectively (see Section 9, Tables 9, 10 for details).

The carbon content of the quartz filters was determined by a thermal method (Evolved Gas Analysis, EGA) where samples are exposed to increasing temperature in an oxygen content controlled carrier gas. In our instrument, the carbon-containing gases evolving as a result of volatilization, decomposition and combustion of the carbonaceous material present in the sample are converted to CO_2 over a CeO_2/CuO catalyst maintained at 900°C. CO_2 is detected by a non-dispersive infrared (NDIR) analyzer. For ACE-2, each sample was heated at a rate of 600°C min^{-1} from 80 to 120, 120 to 220, and 220 to 340°C in a Helium–Oxygen 80:20 mixture (to limit charring), and then from 340 to 650°C in pure Helium. The sample was kept for 1 min at 120, 220 and 340°C, and 2 min at 650°C, leading to 4 separate peaks labelled as OC1.1, OC1.2, OC1.3 and OC2 (Table C). Then oxygen was mixed to the helium flow to obtain a 10% oxygen mixing ratio. The carbon measured during this step we define as black carbon (BC). The detector was calibrated several times a day by injecting in the He carrier gas a known volume of CO_2 using a gas tight micro-syringe. The complete system was calibrated once a day by spiking filters with known amount of C contained in water soluble compounds (e.g., oxalic acid). The precision of the instrument was determined by analysing several aliquots of various samples and was found to be better than $\pm 8\%$. Preliminary results of an intercomparison among 16 laboratories indicate that the accuracy of our instrument is $\pm 20\%$ for total carbon. The accuracy of BC determination is not better than $\pm 60\%$. Due to instrumental problems, OC and BC could not analysed in 9 of the 117 samples collected.

Sampling of carbonaceous particulate matter is subject to various artifacts and an intercomparison study has shown that currently no method can be considered ideal (Hering et al., 1990). Positive sampling artifacts can arise from the trapping of gas phase carbonaceous molecules on the filters, while negative sampling artifacts can result from the volatilization of semi-volatile particulate species from the filters. Both positive and negative artifacts can be reduced or quantified using advanced samplers (Eatough et al., 1993, 1996) but these were not available for the ACE-2 campaign. A simplified technique using back-to-back quartz filters (Fitz, 1990) has been recently used by Novakov et al. (1997, 2000). It is based on the hypothesis that the gas phase organics creating artifacts are only very partially adsorbed by quartz filters, and should therefore be found in the same amount on the back filter. Quantification of positive artifacts based on the analysis of backup filters assumes that there is both no contribution to the backup filter C content from particulate organics volatilized from the front filter, and blank variability is negligible compared to possible artifacts. The average blank for total carbon was 50% of the sample in the batch of pre-fired filters we used for ACE-2. The variability of the blank C content was on average 10% of the mean sample C content. So, at the relatively low carbonaceous species concentrations observed at Tenerife during ACE-2, it is unlikely that the back-to-back filter technique would have improved the carbon data quality. Instead, we have tried to assess, using laboratory tests, the contribution to the thermograms of various volatile and particulate carbonaceous species. This experimental work is described in Section 8. It shows that the OC1.1 probably comprises organic vapors adsorbed on the filter. Heavy hydrocarbons contribute to OC1.3, whereas organic acids and salts evolve as OC2.

Uncertainties remain as to the nature of OC1.2. As a result, we assume the particulate OC amount to be:

$$\mathrm{OC} = 0.5(\mathrm{OC1.2}) + (\mathrm{OC1.3}) + (\mathrm{OC2}). \quad (1)$$

Carbonates were not removed from the samples and could account for up to 15% of OC2 (Section 8). The contribution of the species making up OA was subtracted from OC. We limited charring as much as possible, but we do not have technical means to quantify it. Laboratory tests indicate that charring can result in up to 10% of the OC being converted in BC during the analysis. This figure was used to assess the uncertainty in BC (Tables 9, 10).

As carbonaceous species contain also H, often O, and possibly hetero-atoms, a conversion factor is needed to estimate the mass of carbonaceous aerosol from the mass of carbon quantified by the CO_2 detector. For BC, we assumed that although still present in small amounts (Cachier, 1998), H and O atoms do not contribute significantly to the BC mass and applied a correction factor of 1.0. For organic compounds, the molecular to carbon mass ratio can range from <1.05 (PAHs) to >3.5 (e.g., oxalic acid). However, atmospheric organic aerosol is certainly not made up of only PAHs, or of pure oxalic acid. Conversion factors of 1.4–1.5 have been extensively used (Gray et al., 1986; Wolff et al., 1991; Malm et al., 1994; Eatough et al., 1996), based on the speciation of aerosol carbon performed on a few samples collected at polluted urban sites. Considering that natural organic aerosol species are much more oxidized, Hegg et al. (1997) chose a molecular to carbon ratio of 1.7 for the mix of natural and anthropogenic carbonaceous aerosol collected over the Atlantic Ocean close to America. As Tenerife is also submitted to natural and anthropogenic sources, we used a conversion factor of 1.7 ± 0.3. This range includes the value of 1.4 usually used for polluted areas and the factor of 2 corresponding to a highly oxygenated molecular form $C_3H_4O_2$.

Taking into account (1) the analytical accuracy, (2) the blank variability, (3) the uncertainty in the conversion factor, (4) the possible sampling artifacts, (5) the comparison between the samplers run at the same site and (6) the uncertainty in the sampled air volume, the uncertainties in OC concentrations for the average sample are -97, $+77\%$ and $\pm 74\%$ at PDH and IZO, respectively. BC concentrations were also possibly affected by unquantified charring. The uncertainties in BC concentrations for the average sample are about -250, $+150\%$ at both sites.

The concentrations of the ionic, carbonaceous and mineral aerosol components we quantified were summed up to get the estimate of the submicron aerosol mass concentration from chemical analyses m_{CA}. The overall uncertainties in m_{CA} for

the average sample were −33, +39% and −68, +65% for PDH and IZO, respectively.

2.3. Size distribution and aerosol absorption coefficient measurements

2.3.1. PDH instrumentation. The aerosol absorption coefficient (B_{abs}) was recorded with a 30 min time resolution using an Aethalometer™ (AE-10, MAGEE Scientific). All instruments for particle sizing sampled from the same inlet located at the same height as the PM10 inlets (Van Dingenen et al., 2000). Particle size distributions at 20 ± 10% RH were measured with a 10-min time resolution in the size range 6–500 nm using a Vienna type differential mobility analyser (DMA) equipped with a pre-impactor. The comparison with a condensation particle counter (CPC) indicates that the uncertainty in DMA counting was −10, 0%. The possible error in DMA sizing due to the uncertainty in the air flow rates (±5%) was −7, +5% of the particle diameter. The equivalent mobility diameter as measured by the DMA was considered to be equal to the geometric diameter.

Particle-size distributions for aerodynamic diameters greater than 1 μm were measured using a TSI 33B aerodynamic particle sizer (APS). An intercomparison between the APS used at PDH and IZO carried out at the beginning of the campaign indicated that the uncertainty in APS counting and sizing were ±5% and ±6%, respectively. The APS sizing is affected by the dependence of the correction factor (actual aerodynamic diameter/measured aerodynamic diameter) on the particle density (1.9 ± 0.2) by ±5% (Ananth and Wilson, 1988). Phantom counts were not considered to interfere with < 5μm diameter particle counting. The aerodynamic diameters determined by the APSs were converted to geometric diameters assuming spherical particles and using a standard aerosol density of 1.9 ± 0.2.

2.3.2. IZO instrumentation. The aerosol absorption coefficient (B_{abs}) was measured using a radiance research particle/soot absorption photometer. All the sizing instruments sampled from a common inlet (Van Dingenen et al., 2000) located about 2 meters below the PM10 inlets. Particle size distributions in the size range 7–460 nm were measured in dry conditions (0% RH) with a 10-min time resolution using a Vienna type differential mobility analyser (DMA) identical to the one used it PDH. This DMA compared within ± 2% with the one used at PDH (Van Dingenen et al., 2000). Particle size distributions for aerodynamic diameters greater than 1 μm were measured using a TSI aerodynamic particle sizer (APS33), which was successfully compared to the one used at PDH. The systematic errors in particle sizing and counting are the same as for the instruments used at PDH.

2.3.3. Data processing. The number size distributions were averaged over the filter sampling periods. The gap between the DMA and APS diameter ranges (500–750 nm at PDH, 460–720 nm at IZO) was filled by fitting the DMA bigger mode and APS smaller mode with lognormal distributions. The aerosol volume size distribution was then calculated from the whole number size distribution inferred from DMA and APS measurement (Fig. 3). The full aerosol volume distributions were integrated up to the 50% cut-off of the aerosol sampler, taking into account the impaction efficiency curves of the VIs and the SFUs for PDH and IZO, respectively. To assess the sensitivity of the aerosol volume to the VIs and SFUs' cut-off diameter, their value was varied within the range of uncertainties (Table 11). The sensitivity of the aerosol volume to the sharpness of the sampler cut-off was calculated as the difference between the values of the aerosol volume obtained considering a sharp cut and using the samplers' impaction efficiency curves. The fraction of the aerosol volume derived from the extrapolation of the DMA and APS size distributions was considered to be affected by an uncertainty of up to ±50%.

Taking into account the uncertainties in (1) instrumental counting and sizing, (2) interpolating the DMA and APS distributions, (3) converting aerodynamic to geometric diameter, (4) samplers' cut-off diameters and sharpness, the overall uncertainties of the submicron aerosol volume are −30, +25% and −30, +34% at PDH and IZO, respectively (Table 11). These ranges of uncertainties are comparable with the figures calculated by Quinn and Coffman (1998) who used a chemical model based on thermodynamic equilibrium to convert number to mass distributions for studying aerosol mass closure during ACE-1. The submicron aerosol mass was calculated from the aerosol volume, the dry aerosol density (1.7 ± 0.2) and the aerosol growth factor at the RH recorded in each particle

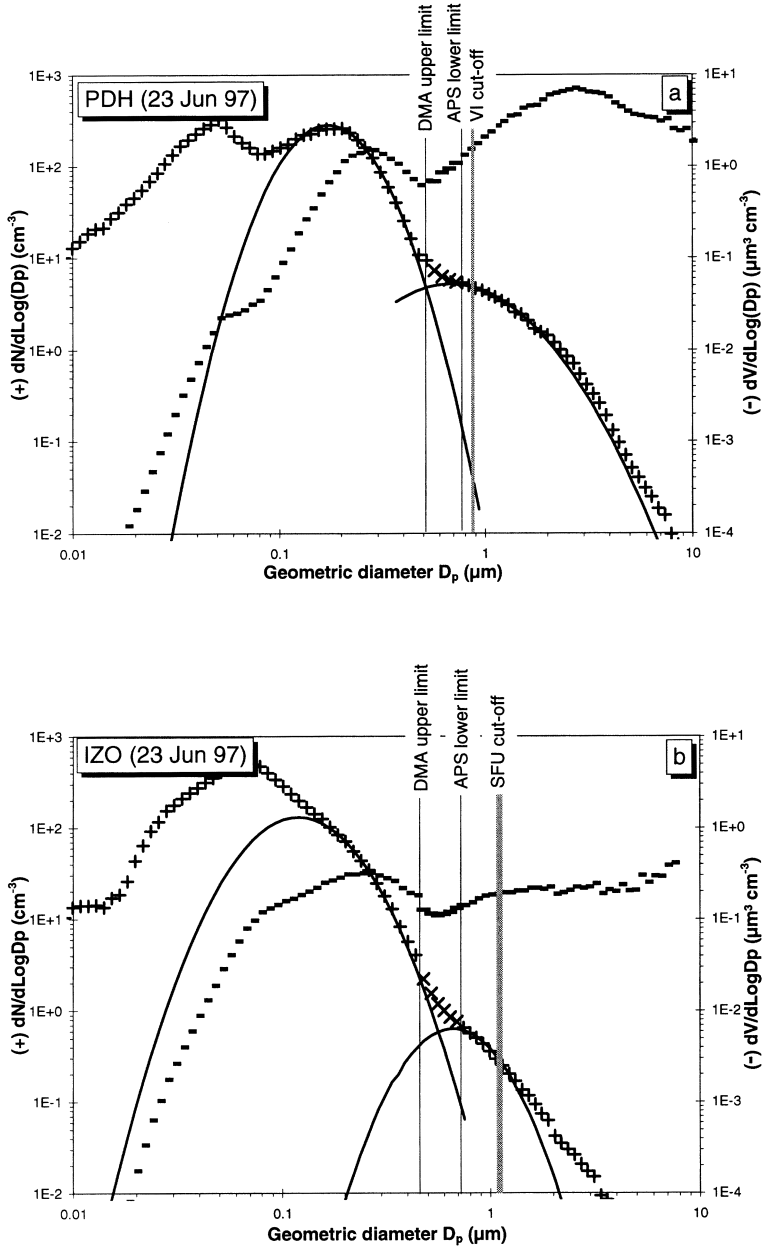

Fig. 3. Example of 12 h-mean number (+) and volume (−) size distibutions at (a) PDH and (b) IZO. Plain lines represent the mono-modal lognormal best fits for the DMA and APS number size distributions. Number size distribution in the gap between DMA and APS (×) is calculated as the sum of these 2 fitted lognormal distributions.

sizer. The overall uncertainty of the aerosol mass concentration calculated from particle size distributions m_{SD} for the average sample was -33, $+28$ and -32, $+36\%$ for PDH and IZO, respectively.

3. Results and discussion

3.1. Mass closure

The first step in a closure experiment is the accurate determination of the uncertainties. Instrumental uncertainties have been rigorously assessed, mainly thanks to intercomparisons. This allows us to identify the main sources of uncertainties associated with each method.

The main source of uncertainty for the gravimetric method (GM) was the variability of the blank masses, which we have attributed to random electrostatic effects on PTFE membranes. This shows the limitation of the gravimetric method when aerosol masses as low as a few micrograms have to be weighed on non-conductive substrates.

The overall uncertainty of the chemical analysis method (CA) was dominated by uncertainties in dust and OC. Again, the uncertainty in dust concentration was mainly due to blank variability. This shows that the method based on ashing and weighing is not precise enough when low volume samplers are used at sites where dust loadings are low. The uncertainty in OC was mainly generated by 2 sources: the sampling artifacts and above all the uncertainty in the molecular-to-carbon ratio. Sampling artifacts can however be reduced by using more complex sampling devices (e.g., Eatough et al., 1996). The uncertainty in the molecular-to-carbon ratio (1.7 ± 0.3) cannot be accurately determined without speciation of the organic carbon component. The range we used is large and encompasses the values recently used in the literature (Malm et al., 1994; Eatough et al., 1996; Hegg et al., 1997). Specific work is needed to determine the molecular-to-carbon ratio of organic aerosol at various sites. At IZO, the uncertainty in m_{CA} was also affected by a possible negative sampling artifact of -2500% in NO_3^- concentrations. Some aircraft observations make us confident in the choice of the central value (see 2.2.2.). However, the use of artifact free samplers (Khlystov et al., 1995) would eliminate this source of uncertainty.

The uncertainty of the method based on aerosol size distribution measurements (SD) is dominated by the uncertainty in the aerosol volume determination. The aerosol volume cannot be expressed as an analytical function of all the parameters. The uncertainty of the aerosol volume was therefore based on a sensitivity analysis in which each of the parameters was varied independently. It appeared that the uncertainties in particle counting, particle sizing, and aerosol volume integration up to the cut-off of the aerosol samplers contribute approximately equally to the overall uncertainty of the aerosol volume. It is interesting to note that the uncertainties in the dry aerosol density (± 0.2) and the particle growth factors (± 0.1), which are the only unmeasured parameters in this calculation account for less than $\pm 12\%$ of the overall uncertainty of the submicron aerosol volume.

To evaluate the mass closure, the submicron aerosol mass (m_i) derived from gravimetric measurements ($i = \mathrm{GM}$), chemical analyses ($i = \mathrm{CA}$), and particle size distributions ($i = \mathrm{SD}$), are compared in regard to the uncertainty associated with each method. The absolute difference $D_{i,j} = |m_i - m_j|$ observed between two methods is compared with the uncertainty in this difference $S(D_{i,j})$ which from formula (D.1) in Section 9 can be estimated from:

$$S(D_{i,j})^2 = S(m_i)^2 + S(m_j)^2. \tag{2}$$

If $m_{i,j}$ is the average of m_i and m_j, the relative uncertainty $\sigma(i, j)$ in the difference $D_{i,j}$ can be evaluated from:

$$\sigma(i, j)^2 = S(Di, j)^2/m_{i,j}^2 = S(m_i)^2/m_{i,j}^2 + S(m_j)^2/m_{i,j}^2. \tag{3}$$

Assuming that m_i and m_j are close enough to the average value $m_{i,j}$, the relative uncertainty in the difference can be approximated by:

$$\sigma^2(i, j) = S(m_i)^2/m_i^2 + S(m_j)^2/m_j^2 = \sigma(m_i)^2 + \sigma(m_j)^2, \tag{4}$$

where $\sigma(m_i) = S(m_i)/m_i$ represents the relative uncertainty in the determination of m_i. $\sigma(D_{i,j})$ has to be compared with the magnitude of the relative difference between two methods i, j:

$$\delta(i, j) = (D_{i,j})/m_{i,j} = |m_i - m_j|/m_{i,j}. \tag{5}$$

Mean absolute relative differences, 95% confidence values of the magnitude of the relative difference, and coefficients of the regression between the methods used to determine the submicron

aerosol mass at PDH and IZO and uncertainties associated with the comparisons are listed in Table 1.

3.1.1. Mass closure in the MBL. Fig. 4a shows the submicron aerosol mass concentration at PDH derived from the 3 methods GM, CA, and SD. For clarity, only the uncertainty of m_{GM} is indicated with error bars. The agreement between the 3 methods is generally good. The correlation coefficient between m_{CA} and m_{GM} and m_{CA} and m_{SD} are 0.87 and 0.90, respectively. The average magnitude relative difference δ(CA, GM) and δ(CA, SD) are 38 and 24%, respectively, i.e., comparable with the uncertainties associated with the comparison of the 2 methods σ(CA, GM) and σ(CA, SD) which are -34, $+41$% and -47, $+48$%, respectively (Table 1). This indicates that the sources of uncertainties are reasonably understood. The agreement between m_{CA} and m_{SD} suggests that the measured aerosol chemical composition is consistent with the independently measured aerosol volume and the parameters listed in Table 11 within the experimental uncertainty σ(CA,SD).

3.1.2. Mass closure in the FT. Fig. 5a shows the submicron aerosol mass concentration at IZO derived from the 3 methods GM, CA, and SD. Only the uncertainty in m_{GM} is indicated with error bars. The agreement between the 3 methods is clearly not as good as for PDH. In particular, GM gives values which are not consistent with the two other methods (CA and SD). However, the mean absolute relative difference δ(CA, GM) = 104% is in line with the uncertainty associated with the comparison of the 2 methods σ(CA, GM) = -102, $+100$%, suggesting that the sources of uncertainties are well understood. The uncertainty associated with GM for IZO samples is so large that it cannot be compared meaningfully with the other methods. The agreement between m_{CA} and m_{SD} is better: ($R^2 = 0.72$, δ(CA, SD) = 28%). δ(CA, SD) is much smaller than the uncertainty associated with the comparison of the 2 methods σ(CA,SD) = -75, $+74$%, which suggests that uncertainties could be overestimated. The results of the chemical analyses are consistent with the measured size distributions and the set of parameters used to convert these distributions to mass concentrations within the experimental uncertainties. It should be noted that the low average discrepancy δ(CA, SD) was achieved without tuning the parameters affected by a large uncertainty (e.g., the molecular-to-carbon ratio in organic aerosol) which were kept equal to the value used for PDH.

In the following discussion, the value assigned to the submicron aerosol concentration is m_{SD} derived from size distribution measurement. The difference ($m_{CA} - m_{SD}$) was attributed to unknown species (unk).

3.2. Air mass characterization

3.2.1. MBL. We used the aerosol absorption coefficient (B_{abs}) to define background and polluted air masses. This parameter was recorded independently of other chemical and physical data. During ACE-2, B_{abs} stayed below 4×10^{-7} m^{-1}

Table 1. *Magnitude of the relative differences, 95% confidence value of the magnitude of the relative differences and coefficient of the correlations between the submicron aerosol mass derived from chemical analyses (m_{CA}), and size distributions (m_{SD}) and gravimetric measurements (m_{GM}); also listed are the uncertainties in the relative difference between m_{CA}, and m_{GM}, and m_{CA} and m_{SD}*

		PDH	IZO
Relative difference between m_{CA} and m_{GM} δ(CA, GM)	average magnitude (%)	38	104
	95% confidence value (%)	60	127
	correlation coefficient R^2	0.87	0.56
	uncertainty (σ) (%)	-34, $+41$	-102, $+100$
Relative difference between m_{CA} and m_{SD} δ(CA, SD)	average magnitude (%)	24	28
	95% confidence value (%)	52	62
	correlation coefficient R^2	0.90	0.72
	uncertainty (σ) (%)	-47, $+48$	-75, $+74$

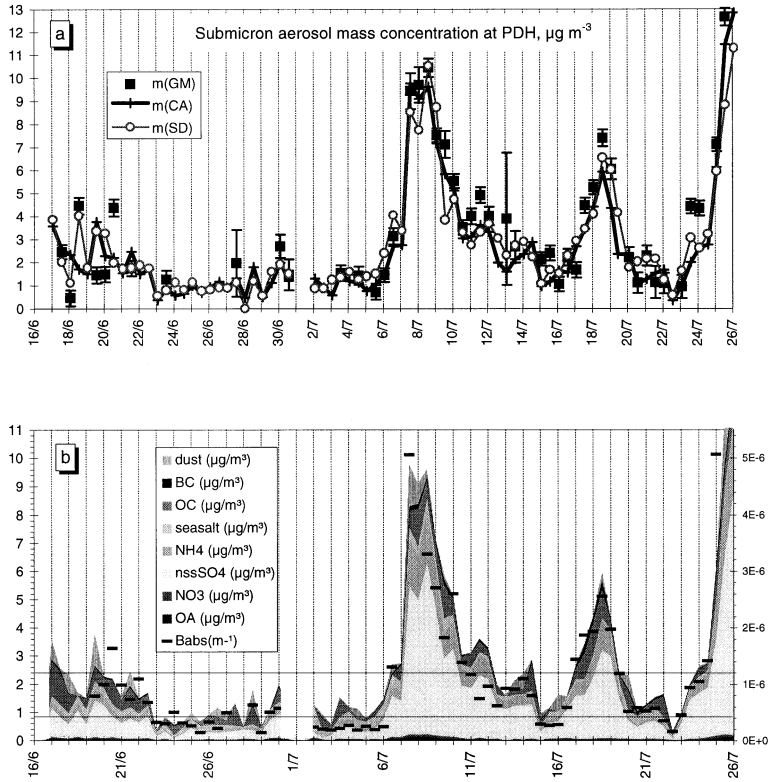

Fig. 4. Temporal variations of (a) the submicron aerosol mass concentration calculated from gravimetric measurements (m_{GM}), chemical analyses (m_{CA}) and size distribution measurements (m_{SD}), and of (b) the submicron aerosol chemical composition and aerosol absorption coefficient (B_{abs}) at PDH. B_{abs} scale is on the right y-axis. Error bars indicate the uncertainty associated with m_{GM}.

for periods of several days (Fig. 4b). This value, corresponding to an equivalent black carbon concentration (EBC) of 20 ng/m^3, was chosen as a threshold characterizing background conditions. Polluted air masses were defined by an enhancement by a factor of 3 in B_{abs} ($B_{abs} > 1.2 \times 10^{-6}$ m^{-1}).

Based on these criteria, we classified the periods 6–10 July, 17–19 July and from 24 July onwards as pollution episodes, whereas most of the samples collected during the periods 23–29 June, and 2–6 July, and 15–16 July were representative of background conditions (Table 2). The data collected on 22 July were not considered because of the local drizzle observed at PDH on this day.

The examination of isentropic 5-day back trajectories (BTs) reaching Tenerife at 975 hPa and 850 hPa shows that the 3 pollution outbreaks were due to transport of pollutants from Europe (e.g., Fig. 1a). This transport was mainly from NW Spain, except on 9–10 July and 24–25 July, when air masses coming from NW Europe travelled to Tenerife above the Atlantic ocean without being affected by Iberia. For background periods, the air masses originated in oceanic regions and had not passed over any continent for at least the 5 previous days (Fig. 1 b,c). We have classified the air masses as Atlantic or Arctic (Table 2) according to the origin of the BTs.

3.2.2. FT. Similarly, the samples collected at IZO were considered as representative of background conditions when they fulfilled the criterion $B_{abs} < 4 \times 10^{-7}$ m^{-1}. The relative maxima in B_{abs} were not always related with high BC concentrations but rather with the presence of dust, which also contributes to light extinction. The nights of 21, 23–26, 30 June and 1, 4–6, 8, 16, 19, 21, 22,

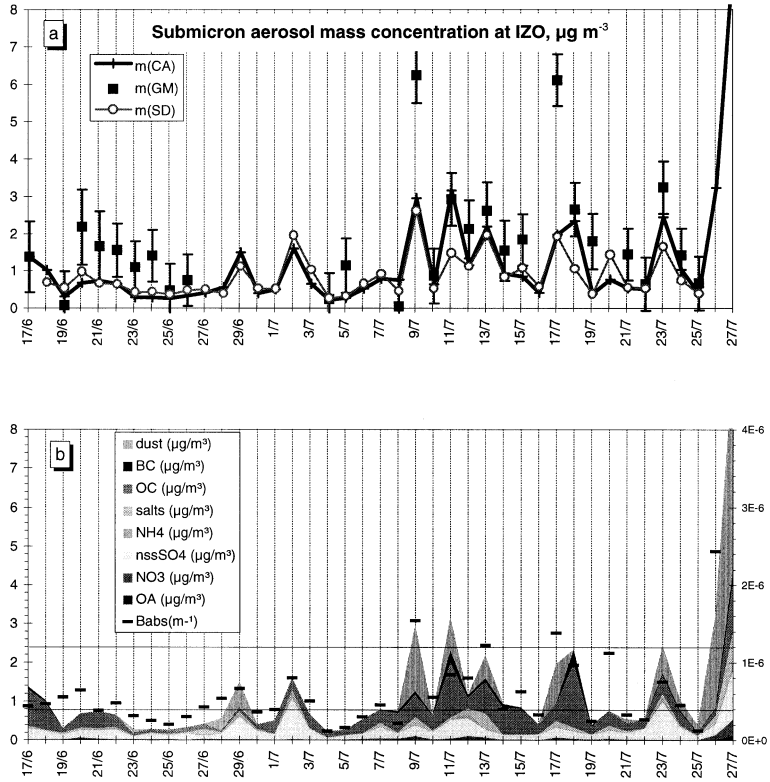

Fig. 5. Temporal variations of (a) the submicron aerosol mass concentration calculated from gravimetric measurements (m_{GM}), chemical analyses (m_{CA}) and size distribution measurements (m_{SD}), and of (b) the submicron aerosol chemical composition and aerosol absorption coefficient (B_{abs}) at IZO. B_{abs} scale is on the right *y*-axis. Error bars indicate the uncertainty associated with m_{GM}.

Table 2. *Classification of the aerosol samples according to the aerosol absorption coefficient and to the origin of the 5-day back trajectories reaching Tenerife at 975 hPa (MBL)*

Sampling period (UTC)	Category	Origin	Traveling over
23 June 08:00–29 June 08:00	background/Atlantic	20–45N, 10–60W	Atlantic Ocean
2 July 20:00–3 July 20:00	background/Atlantic	40–60N, 30–60W	Atlantic Ocean
4 July 08:00–5 July 20:00	background/Arctic	Iceland–Greenland	Atlantic Ocean
6 July 08:00–9 July 20:00	pollution outbreak 1	Iceland–British Isles	Spain
9 July 20:00–10 July 20:00	pollution outbreak 1′	Great–Britain	France
14 July 20:00–15 July 08:00	background/Atlantic	50–70N, 20–40W	Atlantic Ocean
16 July 20:00–19 July 20:00	pollution outbreak 2	Atlantic Ocean	NW Spain
24 July 08:00–25 July 08:00	pollution outbreak 3′	Denmark–Germany	Atlantic Ocean
25 July 08:00–26 July 08:00	pollution outbreak 3	Denmark–Germany	France, NW Spain

and 25 July were classified as background periods whose air masses originated over the Arctic or Atlantic origins (Table 3). On 9, 13, 17, 26 and 27 July, all aerosol chemical and optical properties indicated the presence of light absorbing aerosol. However, the BTs reaching Tenerife at 770 hPa (IZO altitude) suggest advection of Saharan dust on 9 and 26–27 July only.

Table 3. *Classification of the aerosol samples according to the aerosol absorption coefficient and to the origin of the 5-day back trajectories reaching Tenerife at 770 hPa (FT)*

Sampling periods[a]	Category	Origin	Traveling over
22 June	Mixed	North Eastern USA	Atlantic Ocean
23 June	background/Atlantic	35–55N, 35–55W	Atlantic Ocean
30 June–01 July	background/Atlantic	20–30N, 40–50W	Atlantic Ocean
4 July–6 July	background/Arctic	Hudson Bay–Greenland	Atlantic Ocean
9 July	dust outbreak 1	Lybia	Sahara
14 July	Mixed	North Eastern USA	Atlantic Ocean
16, 19, 21, 24 July	background/Atlantic	40–55N, 30–55W	Atlantic Ocean
25 July	background/Arctic	Greenland	Atlantic Ocean
26 July–27 July	dust outbreak 2	Western Sahara	Atlantic Ocean

[a] Dates (e.g., 22 June) stand for sampling periods starting at 20:00 UTC the day before and ending at 08:00 UTC the following day (e.g., 21 June 20:00 to 22 June 08:00).

3.3. *Submicron aerosol chemical composition in background conditions*

3.3.1. FT. The temporal variation of the submicron aerosol chemical composition (night-time samples only) presented generally low concentrations, apart from the 26–27 July (Fig. 5b). The secondary maxima observed on 11 and 18 July (Fig. 5b) were possibly due to contamination by local sources. Accordingly, they have not been considered in the following discussion.

During background conditions, the average sum of the quantified species concentrations m_{CA} was 0.40 μg m^{-3}. Fig. 6a presents the FT aerosol composition based on mean concentrations observed during these periods. Ranges in brackets indicate the uncertainty in the average composition. Fig. 6a suggests that OC was possibly the single major component ($43 \pm 20\%$), while nssSO_4^{2-} accounted for 32 (-5, $+3\%$) of the submicron aerosol mass. The low MSA/nssSO_4^{2-} ratio (0.006 ± 0.004) indicates that DMS oxidation was not a significant source for nssSO_4^{2-} in the FT. The NH_4^+ contribution to the aerosol mass was only 2% and the NH_4^+/nssSO_4^{2-} molar ratio ($< 0.4 \pm 0.1$) indicates that less than 20% of the aerosol could be neutralized by NH_4^+. The contribution of OA, salts, and NO_3^- (not corrected for possible losses, see Subsection 2.2.2.) were comparable (1–2%). Taking into account the upper limit for possible sampling artifacts, the contribution of NO_3^- to the submicron aerosol mass could be up to 44%. Dust accounted for 6 (-4, $+2$)% of the aerosol mass. Single particle analyses suggested alumino-silicates to be the main component of this mineral fraction (Stefaan Hoornaert, personal communication, 1999).

Some BTs show transport in the FT from North America to IZO in 5 days. In these cases (Table 3), the submicron aerosol observed at IZO had the same OC/nssSO_4^{2-} as the aerosol observed offshore of the USA Atlantic coast above 2600 m during TARFOX (Hegg et al., 1997). This suggests a simple dilution of the FT aerosol by a factor of 10 between North America and Tenerife (Table 4). Although the mean OC contribution to the submicron aerosol mass observed at IZO was lower in background conditions (Fig. 6a,b), this difference was not significant with respect to the experimental uncertainties in OC concentrations. This could indicate that the dilution of North American FT aerosol was the main process controlling the North Atlantic FT aerosol in background conditions. TARFOX data suggest an increase in OC/SO_4^{2-} ratio with altitude (Novakov et al., 1997), which may be due to vertical transport through precipitating convective clouds in the boundary layer. Hydrophobic OC (or no water-soluble OC precursors) aerosols would be less efficiently scavenged than hydrophilic species like SO_4^{2-}, MSA, and NH_4^+ (or water soluble SO_2) and therefore reach high altitudes in greater concentrations. Considering the uncertainties in both the TARFOX and ACE-2 data presented here, we can state that these measurements are not inconsistent with the speculation that the FT aerosol observed at IZO in background conditions result from the dilution of continental BL aerosol

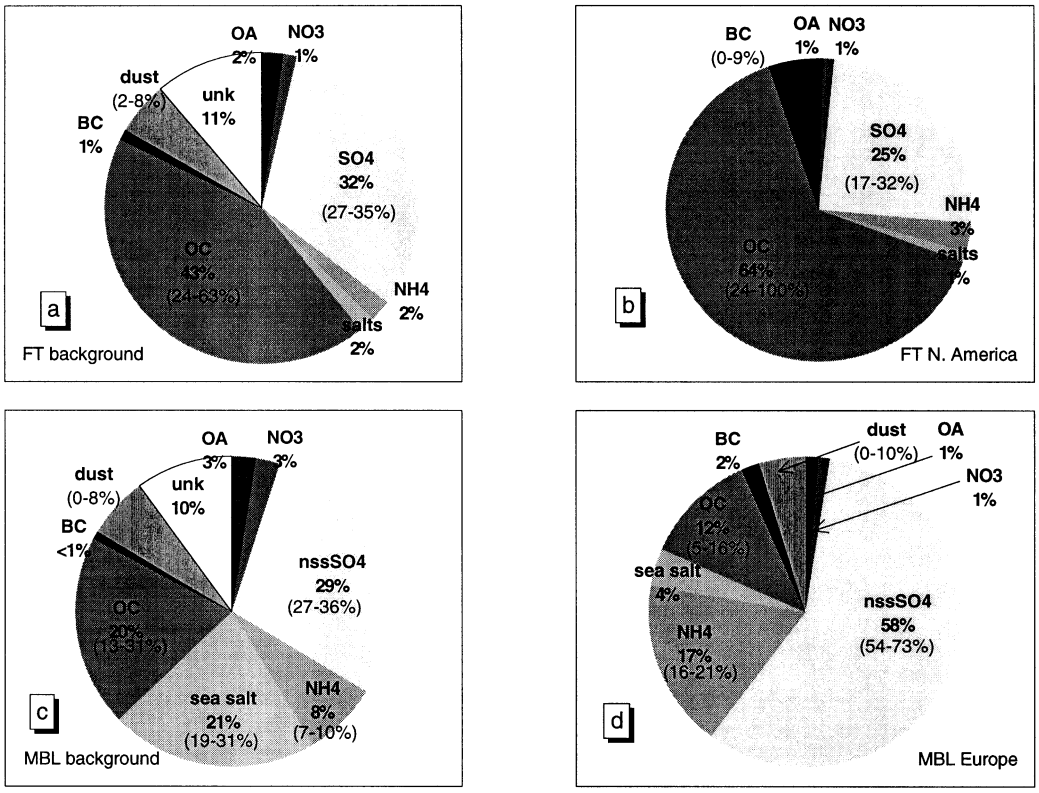

Fig. 6. Mean composition of the submicron aerosol in (a) the FT in background conditions, (b) the FT in North American flows, (c) the MBL in background conditions, and (d) the MBL in European flows. Ranges indicate the uncertainties in the average contributions.

Table 4. *Average concentrations (STP) observed in the FT aerosol samples classified according to Table 3 and compared with literature data; uncertainties in the average concentrations are also indicated*

	$nssSO_4^{2-}$ ($\mu g\ m^{-3}$)	MSA ($ng\ m^{-3}$)	NH_4^+ ($ng\ m^{-3}$)	OC ($\mu g\ m^{-3}$)
average background	0.14 ± 0.01	0.9 ± 0.2	11 ± 1	0.20 ± 0.10
background/ Arctic	0.10 ± 0.02	0.6 ± 0.4	5 ± 2	0.18 ± 0.13
background/Atlantic	0.15 ± 0.02	1.0 ± 0.3	13 ± 2	0.17 ± 0.11
North America	0.19 ± 0.03	1.5 ± 0.8	21 ± 4	0.51 ± 0.32
dust outbreaks	0.61 ± 0.03	0.8 ± 0.4	71 ± 5	0.73 ± 0.20
FT Hobart Flights (ACE-1)[a]	0.19	4.2	43	NM
TARFOX (>2.6 km altitude)[b]	1.8	NM	NM	5.0

[a] Huebert et al. (1998).
[b] Hegg et al. (1997).

Table 5. *Average concentrations (STP) observed in the MBL aerosol samples classified according to Table 2 and compared with literature data; uncertainties in the average concentrations are also indicated*

	$nssSO_4^{2-}$ ($\mu g\ m^{-3}$)	MSA ($ng\ m^{-3}$)	NH_4^+ ($ng\ m^{-3}$)	OC ($\mu g\ m^{-3}$)
average background	0.30 ± 0.05	15 ± 2	82 ± 16	0.21 ± 0.12
background/Arctic	0.32 ± 0.14	18 ± 4	83 ± 40	0.11 ± 0.18
background/Atlantic	0.26 ± 0.7	11 ± 3	77 ± 20	0.24 ± 0.13
pollution outbreaks	3.3 ± 0.40	38 ± 2	1000 ± 120	0.67 ± 0.32
baseline Cape Grim (ACE-1)[a]	0.26	25	21	NM
TARFOX (<1 km altitude)[b]	8.6	NM	NM	7.2

[a] Huebert et al. (1998).
[b] Hegg et al. (1997).

injected into the FT by convective transport through precipitating clouds.

3.3.2. MBL. The temporal variation of the submicron aerosol chemical composition (Fig. 4b) showed low concentrations during the period 22–26 June, and 3 peaks on 7–9 July, 17–19 July and 24–25 July. In background conditions, the average sum of the quantified component concentrations m_{CA} was $1.0\ \mu g\ m^{-3}$. The concentrations of sea salt, $nssSO_4^{2-}$, NH_4^+, MSA, OC and BC were very similar to those observed simultaneously at Sagres, Portugal (Neusüß et al., 2000). On the other hand, concentrations of sea salt, $nssSO_4^{2-}$, and MSA measured simultaneously from the RV Vodyanitskiy were 2–4× higher (Quinn et al., 2000). Fig. 6c shows the average composition of the submicron aerosol during these periods, calculated from mean values (ranges of possible contribution due to uncertainties in brackets). From Fig. 6c it can be seen that on average $nssSO_4^{2-}$ was the major single component. Together with NH_4^+, which was closely correlated with $nssSO_4^{2-}$ ($R^2 = 0.99$), it accounted for 37% (34–46%) of the submicron aerosol mass. The contribution of sea salt was about 20–30%, i.e., not negligible, and comparable to the one of OC (13–31%). Mineral dust accounted for about 6% (0–8%). This contribution is probably overestimated (see Subsection 2.2.2). The residue we observed after ashing the filter was most of the time white, suggesting that it was not Saharan dust. The lack of complementary analysis on this component precludes the assessment of its origin. The low contribution of NO_3^- to the submicron aerosol ($3 \pm 1\%$) was due to its partitioning in favor of supermicron particles where its concentration was on average 10× higher. The concentration of BC was consistent with what would have been calculated from the Aethalometer™ data using a cross section $s = 19\ m^2\ g^{-1}$.

Comparing the mean $nssSO_4^{2-}$ concentration ($0.32\ \mu g\ m^{-3}$) with observations by Huebert et al. (1998) in baseline conditions at Cape Grim during ACE-1 ($0.26\ \mu g\ m^{-3}$) would lead to the conclusion that the North Eastern Atlantic Ocean background is quite clean. However, the average submicron $nssSO_4^{2-}$ concentration observed from the RV Discoverer during ACE-1 was only 0.16 $\mu g\ m^{-3}$. The ratio MSA/$nssSO_4^{2-}$ (0.05 ± 0.01) we observed during ACE-2 is significantly lower than that of 0.1 observed in the Southern Ocean (Table 5). This difference could be explained by a latitude/temperature dependence of the MSA and $nssSO_4^{2-}$ yields from dimethylsulfide (DMS) oxidation (see e.g., Bates et al., 1992) or by the contribution of anthropogenic sources to $nssSO_4^{2-}$ concentration observed in background conditions during ACE-2.

In regard to the experimental uncertainties, the aerosol composition did not significantly differ between periods when BTs originated from the Atlantic and from the Arctic regions (Table 5).

Modelling and experimental studies of size distributions suggested entrainment from the FT to be the main source for particle number in the background MBL (Raes, 1995; Van Dingenen et al., 1999). These authors also suggested that continental aerosol advecting within the MBL would be transformed into a MBL background aerosol mainly by dilution with FT air, deposition and minor modifications due to the condensation

of species of oceanic origin (Van Dingenen et al., 1999). We have tried to simulate the MBL submicron aerosol composition in background conditions using a simple model made of 2 boxes: the MBL above the ocean and the FT on the top of the MBL. Only 3 processes were taken into account: production of particulate OC, MSA, and SO_4^{2-} from sea-surface emitted biogenic compounds (with a 100% aerosol yield and a fixed branching ratio α for MSA), aerosol deposition in the MBL, and entrainment at the FT/MBL interface. The OC, MSA and SO_4^{2-} concentrations in the FT were the mean values observed at IZO in background situations, and the initial OC, MSA and SO_4^{2-} concentrations in the MBL were those of continental polluted MBL aerosol measured during TARFOX (Hegg et al., 1997). The model therefore simulates the evolution towards steady state of a polluted MBL aerosol in presence of the FT aerosol observed in background conditions. The simulated concentrations of OC, MSA and SO_4^{2-} in the MBL (BLOC, BLMSA, $BLSO_4$) are linked to the concentrations of these species in the FT (FTOC, FTMSA, $FTSO_4$) through the equations:

$$\begin{aligned}&\mathrm{HBL}\times \mathrm{d}/\mathrm{d}t(BLOC)\\&\quad = F(\mathrm{C}) - V_g \times \mathrm{BLOC}\\&\qquad + \omega_e \times (\mathrm{FTOC} - \mathrm{BLOC}\end{aligned} \tag{6}$$

$$\begin{aligned}&\mathrm{HBL}\times \mathrm{d}/\mathrm{d}t(BLMSA)\\&\quad = \alpha F(\mathrm{S}) - V_g \times \mathrm{BLMSA}\\&\qquad + \omega_e \times (\mathrm{FTMSA} - \mathrm{BLMSA})\end{aligned} \tag{7}$$

$$\begin{aligned}&\mathrm{HBL}\times \mathrm{d}/\mathrm{d}t(BLSO_4)\\&\quad = (1-\alpha)F(\mathrm{S}) - V_g\\&\qquad \times \mathrm{BLSO_4} + \omega_e \times (\mathrm{FT\ SO_4} - \mathrm{BLSO_4})\end{aligned} \tag{8}$$

where HBL (1000 m) is the height of the MBL and F(C) and F(S) the sea–air fluxes for carbon and sulfur, respectively, corrected for the molecular mass of OC, MSA and SO_4^{2-}. Eqs. (6)–(8) rely on the assumption that the air mass trajectories in the MBL and the FT are parallel for several days, which was the case for the Arctic flows, but only true for 30% of the time in Atlantic flows. The entrainment and the deposition velocity in the MBL (ω_e and V_g) were chosen for consistency with Van Dingenen et al.'s (1999) work (Table 6). With the parameters listed in Table 6, the calculated concentrations are in quasi steady state and independent of the initial MBL aerosol composition after $\sim$10 days (Fig. 7).

The parameters α, F(S) and F(C) were fitted to give agreement between the measured and the calculated steady state concentrations of OC, MSA and SO_4^{2-} in the MBL. The best fit was

Table 6. *Prescribed and fitted parameters, outputs of the computer simulation and mean concentrations measured at PDH in background conditions; extremum fitted parameters result from fits considering extremum average concentrations in the FT and the MBL calculated as averages* $\pm$ *uncertainty in the averages*

			Best fit	Extrema	
Prescribed parameters	entrainment	($cm\ s^{-1}$)	0.65	0.65	0.65
	deposition	($cm\ s^{-1}$)	0.10	0.10	0.10
	$FTSO_4$	($\mu g\ m^{-3}$)	0.14	0.12	0.15
	FTMSA	($ng\ m^{-3}$)	0.90	0.70	1.10
	FTOC	($\mu g\ m^{-3}$)	0.20	0.10	0.30
Fitted parameters	S sea-air flux	($\mu mol(S) m^{-2}\ d^{-1}$)	1.3	1.8	1.1
	MSA yield	(%)	8	5	10
	C sea-air flux	($\mu mol(C)\ m^{-2}\ d^{-1}$)	1.0	7.0	0
Outputs	$BLSO_4$	($\mu g\ m^{-3}$)	0.30	0.37	0.28
	BLMSA	($ng\ m^{-3}$)	15	13	17
	BLOC	($\mu g\ m^{-3}$)	0.21	0.31	0.26
Concentrations measured at PDH	$nssSO_4$	($\mu g\ m^{-3}$)	0.30	0.37	0.28
	MSA	($ng\ m^{-3}$)	15	13	17
	OC	($\mu g\ m^{-3}$)	0.21	0.31	0.07

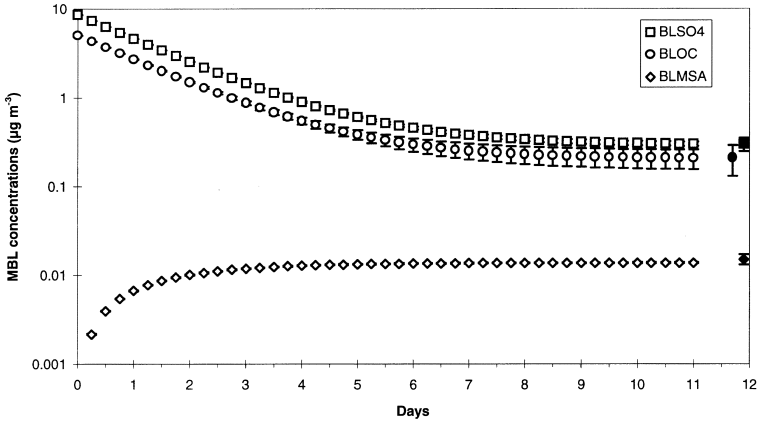

Fig. 7. Simulated evolution of MBL concentrations of SO_4, MSA and OC resulting from deposition, accumulation of condensable species from oceanic origin, and dilution by FT air with an aerosol compostion as observed at IZO in background conditions. Unceratinties in the simultation output due to experimental uncertainties in FT concentrations are shown. Error bars are smaller than symbols for SO_4^{2-} and MSA. Black symbols at $t \approx 12$ days represent the mean values actually measured at PDH. Experimetal uncertainties in these values are also shown.

found with a particulate carbon flux of 1.0 µmol(C) m^{-2} d^{-1} which is reasonable (Alex Guenther, personal communication, 1999), a sulfur flux of 1.3 µmol(S) m^{-2} d^{-1}, consistent with measurements performed during ACE-2 (T. Bates, personal communication, 1998) and a yield of MSA of 8% in line with the temperature dependent MSA/nss SO_4^{2-} ratio calculated by Bates et al. (1992). Taking into account the experimental uncertainties in OC, nssSO_4^{2-} and MSA concentrations (in the FT and MBL) only, the model and the data are still consistent with sea-air carbon and sulfur fluxes of 0–7 and 1.1–1.8 µmol m^{-2} d^{-1}, respectively (Table 6).

This simulation exercise indicates that the aerosol chemical compositions we observed in the FT and the MBL are not inconsistent with the hypothesis that entrainment of submicron aerosol from the FT is the main source of particles in the MBL, where they grow through accumulation of condensable species of biogenic origin.

3.4. The aerosol outbreaks

Aerosol outbreaks were observed in both the FT and the MBL (Figs. 4, 5). These were associated with transport of Saharan and European aerosol, respectively.

3.4.1. The Saharan outbreaks in the FT. Only 2 aerosol outbreaks in the FT were undoubtedly due to the advection of Saharan aerosol: a minor event on 9 July, and a major event starting at the end of the campaign on 26–27 July.

This last event was comparable in magnitude with what was observed during the pre-ACE-2 campaigns in July 1995 and 1996, with a submicron aerosol mass concentration reaching 10 µg m^{-3}. These Saharan outbreaks were mainly characterized by high dust loadings, but enhanced nssSO_4^{2-} were observed as well (Table 4). The mean OC concentration was 3 × as high as during background conditions, which is significant in regard to the experimental uncertainties in OC. During the dust events, nssSO_4^{2-} was likely not only of Saharan origin: Alpine glacier ice-cores (Schwikowski et al., 1995) and IC analyses of Saharan sand fine grain samples suggest that the SO_4^{2-}/Ca^{2+} mass ratio should be about 0.4–0.6 in pure Saharan dust. The SO_4^{2-}/Ca^{2+} ratio observed at IZO during the dust events ranged from 1.8 ± 0.8 to 2.9 ± 1.2. As these values should be considered as lower limits due to the uncertainties in Ca^{2+} determination (Section 6, 7), this suggests that at least 80% of the FT nssSO_4^{2-} observed during Saharan outbreaks was probably of anthropogenic origin.

3.4.2. The European outbreaks in the MBL. As shown in Fig. 4, three major aerosol outbreaks were observed in the MBL. They resulted from

fast transport of pollutants from Europe in the MBL (Table 2, Fig. 1a). These pollution events were characterised by an increase of one order of magnitude in the submicron aerosol concentration. The average composition of the pollution aerosol observed at PDH is shown in Fig. 6d (ranges of possible contributions taking into account experimental uncertainties are indicated in brackets). Fig. 6d shows that nssSO_4^{2-} was undoubtedly the main submicron aerosol component. The sum of nss$SO_4^{2-} + NH_4^+$ made up 70–84% of the submicron aerosol mass. The relative contribution of OC (5–16%) was not significantly smaller than during background conditions, whereas the contribution of OA was, despite the enhancement of the absolute mass concentration of this component during the pollution peaks. In particular, submicron MSA increased significantly during pollution peaks (Table 4). The sea salt submicron concentration was unchanged ($0.23\ \mu g\ m^{-3}$) in the pollution events, which suggests that the balance between sinks and sources for species emitted from the sea surface remained relatively constant. The increase in MSA concentration was therefore possibly due to changes in DMS atmospheric chemistry (Mangoni and Putaud, 1998). The contribution of NO_3^- to the submicron aerosol mass was negligible, due to its partitioning during atmospheric transport onto coarse aerosols: in the supermicron fraction, NO_3^- concentration averaged $1.6\ \mu g\ m^{-3}$ during the pollution outbreaks.

The predominance of nssSO_4^{2-} with respect to OC in the submicron pollution aerosol is rather surprising. Such a composition is unlikely to result from the fast transport of urban aerosol from Europe to PDH as SO_4^{2-} and organic carbon account on average for about 30% of the submicron mass in urban aerosol (Heintzenberg, 1989). An additional source for SO_4^{2-} would be needed to increase its mass fraction on the way between urban areas and Tenerife. The oxidation of SO_2 during atmospheric transport over the ocean could be this source. However, a simple calculation, using a very low SO_2 dry deposition rate ($0.5\ cm\ s^{-1}$), shows that unrealistically high initial SO_2 concentrations (>50 ppbv) would be needed for this process to contribute significantly to the SO_4^{2-} levels observed at Tenerife. A source close to Tenerife that produces specially high amounts of sulfur compounds could explain this unusually high fraction of SO_4^{2-} in the aerosol. EMEP inventories show that ship traffic along the Portuguese coast is a significant source of sulfur (Berge, 1997). The same document also indicates that the Spanish power plants of As Pontes and Meirama (43°N, 8°W) make up the second largest point source of SO_2 in Europe (360×10^9 gS/yr). However, the SO_4^{2-} contribution stayed high even when the 5 day back trajectories did not pass over NW Spain (outbreak 1′ and 3′). Since back trajectories only describe the centerline of an advected air mass, trajectories do not take into account the vertical and horizontal dispersion (Kahl, 1993) of advected air masses. Thus a back trajectory may not pass over all of the sources that contribute to a particular air mass.

4. Conclusion

A rigorous assessment of the uncertainties involved in the determination of the submicron aerosol mass concentrations based on gravimetric measurements (GM), chemical analyses (CA), and size distributions measurements (SD) allowed us to determine how accurately quantifying the organic, inorganic and mineral dust components of the submicron aerosol could lead to a full description of the submicron aerosol observed at PDH and IZO during ACE-2. This mass closure experiment showed that the sum of the species concentrations we measured (m_{CA}) was consistent with the aerosol mass concentrations calculated from the particle size distributions (m_{SD}) within experimental uncertainties of -47, $+48$% and -75, $+74$% for PDH and IZO, respectively. The overall uncertainty of m_{CA} would be greatly reduced by using artifact free samplers, determining the molecular-to-carbon ratio in organic aerosols, and quantifying more accurately the aerosol mineral dust. The accuracy of m_{SD} is about equally affected by the uncertainties in particle counting, particle sizing, and in the aerosol density and growth factor, needed to derive the aerosol mass concentration from the volume size distribution.

Taking into account these uncertainties, we found no significant difference between OC concentrations in the FT and MBL in background conditions, whereas SO_4^{2-}, NH_4^+ and sea-salt concentrations were significantly higher in the MBL. Based on a comparison with data obtained during

the TARFOX experiment, we suggest that the FT aerosol observed in the background conditions probably comes from the transport of BL continental aerosols in the FT after having passed through precipitating convective clouds. The difference in aerosol composition between the FT and MBL background aerosol is not at odds with the hypothesis that entrainment is the main process controlling the MBL aerosol size distribution. A model simulation showed that the SO_4^{2-}, MSA and OC concentrations observed in the MBL in background conditions are consistent within experimental uncertainties with this entrainment hypothesis. Nevertheless, additional work such as speciation of OC and measurements of stable S isotopes in the FT and the MBL would provide important data to further test this hypothesis.

Aerosol outbreaks characterized by increases in the submicron aerosol concentration by one order of magnitude were observed in both the FT and the MBL. The 5 day back trajectories for these outbreaks indicate transport of mineral dust from North Africa and pollution aerosol from Europe, respectively. The levels of $nssSO_4^{2-}$ observed in the dust outbreaks in the FT indicate the presence of pollution aerosol mixed with mineral dust. The origin and interaction of this mixed aerosol merits further investigation. The contribution of $nssSO_4^{2-}$ to the pollution aerosol reaching Tenerife in the MBL was surprisingly high. Much of this SO_4^{2-} may have been produced by two large power plants located in the Northwest of Spain. Long-term aerosol sampling at Sagres and Cabo da Roca (Portugal), and Punta del Hidalgo (Tenerife) has been carried out for 3 years. These data will be useful in the assessment of the representativeness of these elevated aerosol SO_4^{2-} concentrations.

5. Acknowledgements

We are thankful to T. Bates and P. Quinn for their comments on the manuscript. This research is a contribution to the International Global Atmospheric Chemistry (IGAC) Core Project of the International Geosphere–Biosphere Programme (IGBP) and is part of the IGAC Aerosol Characterization Experiments (ACE). It has been supported by the EC contract ENV4-CT95-0140 (FREETROPE).

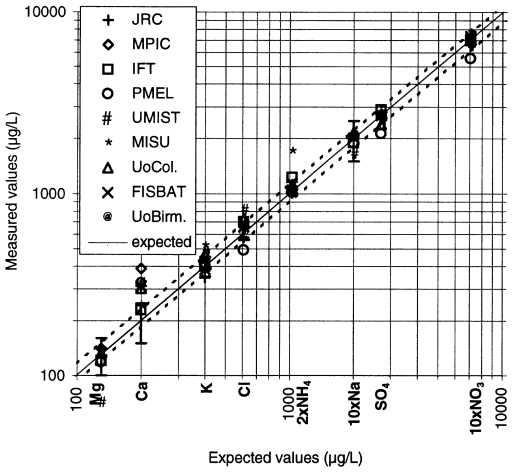

Fig. 8. Results of the intercomparison regarding main ion analysis. The dotted lines represent a 10% deviation to the expected values.

6. Appendix A

IC intercomparison

A first intercomparison among the ACE-2 participants was carried out in 1997. Standard solutions and spiked quartz and PTFE filters were analysed to assess possible discrepancies in extraction techniques and analytical methods (ion chromatography, capillary electrophoresis). This intercomparison showed that the principal source of disagreement among us was the analysis of the liquid samples. A second set of synthetic rainwater standards was distributed to the participants at the time they were analysing their ACE-2 samples. The results of this second exercise are plotted on Fig. 8. All the participants found the expected value to within $\pm 10\%$ for all the species of the solution except for Ca^{2+}, for which almost all of us found a concentration 1.5 higher than the reference value.

The results of this intercomparison can be considered as a measure of the accuracy of our IC analyses. Several tests of reproducibility showed the precision of our IC instrument to be better than $\pm 2\%$. These data are used to assess the uncertainty in IC analyses of the ionic compounds listed in Tables 9, 10.

7. Appendix B

Sampler intercomparison

The ionic species, carbonaceous species and mineral dust were analysed from different filter types (PTFE, Quartz and Whatman 41, respectively) placed in 3 samplers located side by side at each of the 2 sites (PDH and IZO). Since the results from the 3 samplers of each site had to be combined to determine the aerosol composition, it is useful to know how they compared.

At PDH, samples were collected on PTFE and Quartz filters in two identical virtual impactors (VI). These 2 VIs compared well with a regression slope = 1.19 for $nssSO_4^{2-}$ concentrations (Fig. 9a), but the agreement was not so good for Na^+ (slope = 1.41, Fig. 9b). The systematic difference observed for $nssSO_4^{2-}$ suggests inaccurate measurements of the flows in one of the VIs. The slope of the regression is greater for Na^+ than for $nssSO_4^{2-}$, indicating that the "1 μm" cut-off was larger in the VI sampling with quartz filters than the VI sampling on PTFE filters. The "noise" in the Na^+ regression is attributed to uncertainties related to IC analyses and blank variability. The comparison of the samplers indicated possibly systematic errors in sampling. They are considered as such for the uncertainty calculations in Table 9.

The stacked filter unit (SFU) used at PDH for the analysis of mineral dust had a 1.6 μm aerodynamic cut-off versus 1.26 μm cut-off for the VIs. We found 2× more sea salt in the SFU samples than in the VI samples. Since mineral dust, like sea salt, is usually concentrated in the coarse aerosol fraction, we assigned an uncertainty of −100% to the dust amounts detected at PDH due to the possible contribution of supermicron dust particles to the aerosol fine fraction collected with the SFU (Table 9).

As mentioned in Subsection 2.2.2, we did not analyse for ionic species the quartz filters sampled at IZO. The whole quartz filters were used for OC analyses to maximise the amount of OC to be analysed. The fine aerosol fraction collected on quartz and Whatman 41 filters using SFUs compared very well during the 1996 campaign at IZO (e.g., for SO_4^{2-}: slope = 0.98, $R^2 = 0.97$). The $nssSO_4^{2-}$ concentration in the fine aerosol fraction collected in SFU samples on PTFE and Whatman 41 filters differed on average by only 6% during ACE-2 (Fig. 10a). However, Ca^{2+} in the same samples differed by 36% (Fig. 10b). We used this as an estimate of uncertainty in the determination of "salts" and "dust" at IZO (Table 10). The systematic differences between samplers were considered as non-stochastic errors in the uncertainty calculations (Table 10).

8. Appendix C

Carbonaceous aerosol concentration determination

8.1. Discrimination between adsorbed gaseous and particulate carbon

The C analysis steps and nomenclature, blank to sample ratios, representative species and the

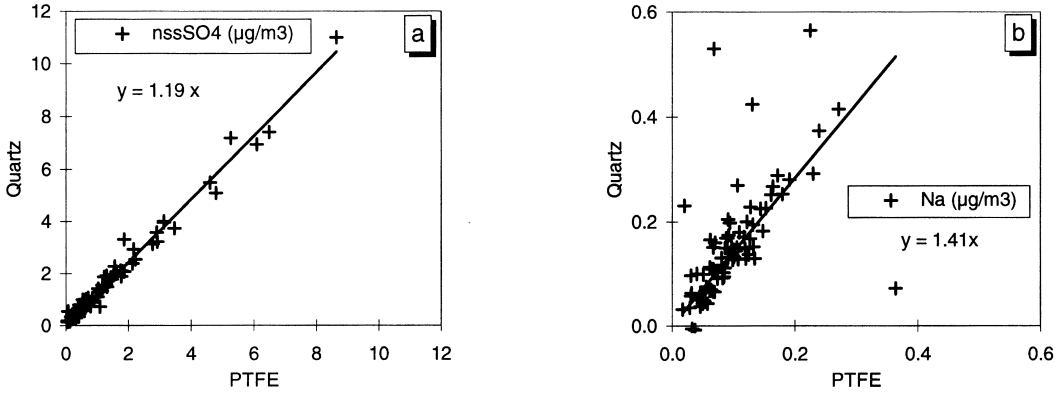

Fig. 9. Comparison of (a) $nssSO_4^{2-}$ and (b) Na^+ concentrations measured with the two virtual impactors sampling at PDH on PTFE and quartz filters, respectively.

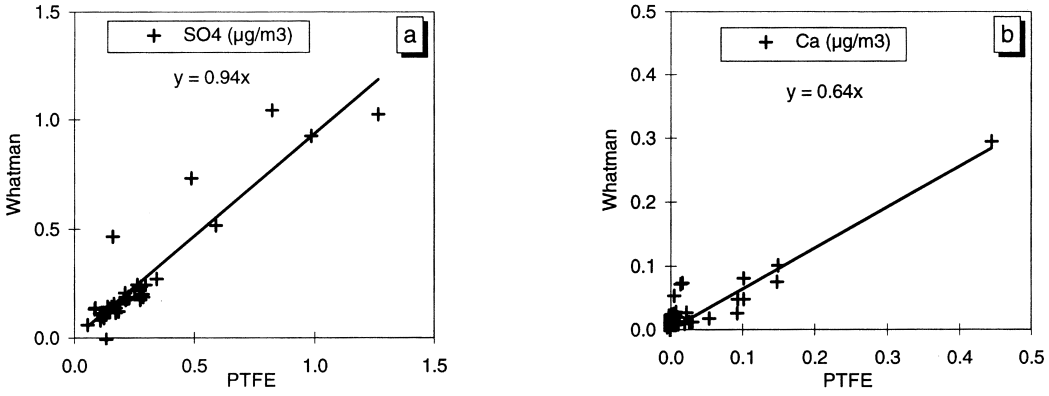

Fig. 10. Comparison of (a) SO_4^{2-} and (b) Ca^{2+} concentrations measured with the stacked filter units sampling at IZO on PTFE and Whatman 41 paper filters, respectively.

Table 7. *Characteristics of the 5 carbonaceous fractions resolved during carbon analysis*

C fraction	Temperature °C	Carrier gas O_2:He mixture	Mean blank to sample ratio	Contributing species	Considered as particulate C
OC1.1	<120°C	20:80	100%	HCHO, limonene	0%
OC1.2	120–220°C	20:80	50%	Anthracene vapor, benzoic acid	50%
OC1.3	220–340°C	20:80	50%	Coronene	100%
OC2	340–650°C	0:100	50%	Pinic acid, MSA, oxalate, $CaCO_3$	100%
BC	650–700°C	10:90	30%	Amorphous C	
				NOT graphitic C	100%

fraction regarded as particulate carbon in the 5 OC fractions resolved during the C analysis are listed in Table 7.

- *OC1.1.* Fitz (1990) recommends heating particulate OC samples to 120°C prior to analysis to remove adsorbed organic vapor from the samples. We applied this treatment for 1 min as a first analytical step in the analysis of the OC1.1 fraction. The mean blank level (0.7 ± 0.5 µgC) was 90% of the mean sample (0.8 ± 0.6 µgC). The OC1.1 fraction was therefore not considered as resulting of the volatilization of atmospheric particulate compounds.
- *OC1.2.* The OC1.2 fraction evolving from the samples between 120 and 220°C was on average twice as high as from the blanks (3.0 ± 1.6 versus 1.6 ± 0.5 µgC). However, analyses of freshly pre-fired filters exposed to saturation pressure vapors of anthracene at room temperature produced signals in the 120–220°C temperature range. Thus organic gases adsorbed onto quartz filters can contribute to the OC1.2 fraction. On the other hand, non-volatile species such as benzoic acid contribute to OC1.2 as well. Novakov et al. (1997) considered what volatilizes between 120 and 220°C to be, at least in part, due to positive artifacts. Therefore, we considered an arbitrary fraction of 50% of OC1.2 to be particulate carbon. Note that the mean contribution of OC1.2 to total OC was 31 ± 7%. This correction introduces an uncertainty in the total OC concentration of 12–19%.
- *OC1.3.* The OC1.3 fraction was on average $1.5\times$ higher in samples than blanks (1.9 ± 0.9 vs. 1.2 ± 0.4). Laboratory tests showed a compound such as coronene (PAH, M = 300, BP = 525°C) to be part of OC1.3. The boiling point of coronene is so high that this compound is not volatile at ambient temperatures. Therefore, 100% of OC1.3 is considered to be particulate carbon.
- *OC2.* OC2 was, on average, $2.2\times$ higher in samples than blanks (3.8 ± 2.7 versus 1.7 ± 0.5). Laboratory tests showed most organic acids (e.g., pinic, pinolic) and all the organic acid

salts (e.g., MSA, acetate, oxalate) tested to be part of the OC2 fraction. Thus the OC2 fraction would be made up of primarily water soluble species as well as contain most of those water soluble organic compounds. These molecules are not volatile. This is particularly true in atmospheric conditions where they can exist in acid salt form. Therefore, we consider the OC2 fraction 100% particulate.

8.2. *Discrimination between OC and carbonates*

In our instrument, pure $CaCO_3$ and Na_2CO_3 (precipitates) are decomposed in a He flow at 650° and 750°C, respectively. $CaCO_3$ could therefore contribute to the OC2 peak. Carbonates are usually removed from the samples prior to carbon analysis by exposure to acidic (HCl) fumes. Treatment with acidic fumes reduced the OC2 peak and the other OC peaks by as much as 15% in samples collected at PDH and IZO during periods dominated by clean, polluted and mineral dust conditions. Chow et al. (1990) suggested that organic acids could be lost as a consequence of acidic treatment. We concluded that the acidic treatment was not relevant for samples collected at Tenerife. It was not performed and consequently, the OC2 fraction may include up to 15% of carbonates. Carbonates are therefore included in the chemical mass balance, but not resolved from OC.

8.3. *Discrimination between OC and BC*

The carbonaceous fraction labelled BC evolved at $T \leqslant 650$°C in a 1:9 O_2:He mixture. Tests performed with amorphous black carbon (Corax N220, Degussa) deposited on quartz particles showed that up to 10% of the total carbon evolved in each of the OC1.3 and OC2 fractions. It is not possible to determine if this was due to impurities in the black carbon standard or to the partial volatilization of BC at $T \leqslant 340$°C in 1:4 O_2:He or at $T \leqslant 650$°C in pure Helium. Graphitic carbon evolves in our instrument at $T > 700$°C in He and O_2. Therefore, the BC fraction observed in Tenerife samples was not graphitic carbon. There is no evidence that the BC fraction coincides exactly with the black carbon species defined from its absorption properties.

Charring of OC into BC during OC analysis has been previously reported (Chow et al., 1993). We observed charring in a range of pure organic chemicals such as benzoic acid, pinic acid, and coronene. The BC peak represented up to 10% of the total C mass. Charring should not happen at $T < 340$°C in He/O_2 (Thomas Kuhlbusch, personal communication, 1996). However, we had no explicit way to determine whether charring took place during the 350–650°C step in He with aerosol samples. The determination of OC was likely unaffected because on average OC was 7× larger than BC. However, the charred OC could have accounted for 82–87% of the mean BC values. The BC concentrations measured by this method is highly uncertain at non-urban sites.

9. Appendix D

Calculation of the uncertainties related to the chemical mass closure

If $y = f(x_1, x_2, ..., x_n)$ is a function of n non-correlated parameters $(x_1, x_2, ..., x_n)$, the variance $S(y)^2$ may be approximated according to the law of propagation of errors by:

$$S(y)^2 = (\mathrm{d}f/\mathrm{d}x_1)^2 S(x_1)^2 + (\mathrm{d}f/\mathrm{d}x_2)^2 S(x_2)^2 + ... + (\mathrm{d}f/\mathrm{d}x_n)^2 S(x_n)^2 \quad (9.1)$$

where $(\mathrm{d}f/\mathrm{d}x_i)$ represents the partial derivative of f with respect to x_i applicated to $(x_1, x_2, ..., x_n)$, and $S(x_i)$ is the uncertainty of parameter x_i.

Formula (9.1) combines absolute uncertainties. It was used to calculate the uncertainty of m_{GM}

Table 8. *Relative uncertainties $S(x_i)/x_i$ (%) in the parameters associated with the determination of the aerosol mass concentration by gravimetry m_{GM} for the average sample; these uncertainties are combined according to the law of propagation of errors to assess the uncertainty in m_{GM} (see text)*

	Relative uncertainty PDH	IZO
m_{GM} overall uncertainty (%)	−10, +12	±76
due to:		
weighing (%)	3	11
blank variability (%)	±10	±86
RH in glove box (%)	negligible	negligible
air volume (%)	−2, +6	±11

Table 9. *Relative uncertainties $S(x_i)/x_i$ (%) in the parameters associated with the aerosol chemical composition of the average sample at PDH; these uncertainties are combined according to the law of propagation of errors to assess the uncertainty in m_{CA} (see text)*

	OA	NO_3^-	$nssSO_4^{2-}$	NH_4^+	sea salt	OC	BC	dust	sum = m_{CA}
overall uncertainties due to analyses	−14, +28	−62, +12	−12, +32	−11, +32	−11, +54	−97, +77	−270, +150	−350, +250	−33, +39
analytical accuracy	±10	±10	±10	±10	±10	±20	±60	±7	
blank variability	±7	±9	±4	±3	±3	±8	±12	±29	
molecular/carbon ratio						±18			
charring							−87, 0		
sampling									
air volume	−2, +6	−2, +6	−2, +6	−2, +6	−2, +6	−6, +0	−6, +0	−1, +11	
sampling artifacts		−40, 0		−2, 0		±21			
sampler intercomparison	0, +13	−33, 0	0, +19	0, +19	0, +41	−13, 0[a]	−19, 0[b]	−100[c], 0	

[a] Estimated by analogy with OA.
[b] Estimated by analogy with $nssSO_4^{2-}$.
[c] Estimated by analogy with sea salt.

Table 10. *Relative uncertainties $S(x_i)/x_i$ (%) in the parameters associated with the aerosol chemical composition of the average sample at IZO; these uncertainties are combined according to the law of propagation of errors to assess the uncertainty in m_{CA} (see text)*

	OA	NO_3^-	$nssSO_4^{2-}$	NH_4^+	salts	OC	BC	dust	sum = m_{CA}
overall uncertainties due to:									
analyses	−69, +63	−40, +1500	−22, +16	−23, +17	−100, +80	±74	−250, +150	−390, +350	−68, +65
analytical accuracy	±10	±10	±10	±10	±10	±20	±60	±6	
blank variability	±42	±17	±5	±10	±28	±11	±11	±19	
molecular/carbon ratio						±18			
charring							−82, 0		
sampling									
air volume	±11	±11	±11	±11	±11	±10	±10	±10	
sampling artifacts		+2500, 0				±21			
samplers intercomparison	−6, +0[a]	−6, +0[a]	−6, +0	−6, +0[a]	−36, +0[b]	−6, +6[a]	−6, +6[a]	−0, +36[b]	

[a]Estimated by analogy with $nssSO_4^{2-}$.
[b]Estimated by analogy with Ca^{2+}.

Table 11. *Uncertainties in the parameters associated with the determination of the submicron aerosol mass from particle size distributions m_{SD}; these uncertainties are combined according to the law of propagation of errors to assess the uncertainty in m_{SD} (see text)*

	Relative uncertainty	
	PDH	IZO
m_{SD} overall uncertainty (%)	−33, +28	−32, +36
due to uncertainties in:		
aerosol density at 0% RH (%)	±12	±12
growth factor at particle sizers' RH (%)	±5	0
aerosol volume at sizers' RH (%)	−30, +25	−30, +34
including:		
particle counting		
DMA counting (from comparison with CPC) (%)	−10, 0	−10, 0
APS counting (from intercomparison) (%)	±5	±5
interpolation between DMA and APS (%)	±50	±50
particle sizing		
DMA sizing (due to 5% uncertainty in flow rate) (%)	−7, +5	−7, +5
APS sizing (from intercomparison and density dependent correction factor) (%)	±8	±8
conversion of APS data from aerodynamic to geometric diameter (%)	±5	±5
Volume size distribution integration (%)	±10	−4, +12
from		
aerosol sampler S curve shape (%)	±9	±1
50% cut-off at particle sizer RH (μm)	0.85 ± 0.09	1.05
from		−0.11, +0.20
growth factor at particle sizers' RH	1.05 ± 0.05	1.00
		1.05
growth factor at ambient RH (μm)	1.38 ± 0.1	−0.05, +0.15
50% cut-off at ambient RH (μm)	1.12 ± 0.06	1.11
from		−0.10, +0.13
sampler 50% aerodynamic cut-off, μm	1.26 ± 0.05	1.40 ± 0.10
density at ambient RH	1.27 ± 0.10	1.60
from		−0.19, +0.31
aerosol submicron density at 0% RH	1.7 ± 0.2	1.7 ± 0.2
growth factor at ambient RH (μm)	1.38 ± 0.1	1.05
		−0.05, +0.15

(Table 8) and m_{CA} (Tables 9, 10) for the average sample by combining the random errors in the parameters and using the average parameter values observed at PDH and IZO. Uncertainties associated with the conversion of organic carbon to organic compound concentrations and uncertainties underlined by the samplers' intercomparisons were considered to be possibly systematic. They were therefore simply added in a conservative way.

Formula (9.1) was used also for the calculation of the uncertainty of m_{SD} when aerosol properties were calculated from independent parameters using an analytical formula (formula 9.2–9.4):

- aerosol density at ambient RH, d_a:

$$d_a = (d_0 + (GF_a^3 - 1)d_w)/GF_a^3, \quad (9.2)$$

where d_0 is the aerosol density at 0% relative humidity, d_w is the density of water (= 1.0) and GF_a the aerosol growth factor at ambient relative humidity.

- sampler 50% cut-off geometric diameter at ambient RH, D_a:

$$D_a = D_{aero}/(d_a)^{1/2}, \quad (9.3)$$

where D_{aero} is the sampler aerodynamic cut-off.

- sampler 50% cut-off at the particle sizer RH,

D_s:

$$D_s = GF_s \times D_a / GF_a, \quad (9.4)$$

where GF_s is the aerosol growth factor at the sizer's RH.

D_s is the upper limit up to which the volume size distributions have to be integrated.

To assess the sensitivity of the aerosol volume $V(D_s)$ to the sampler cut-off, D_s was varied within its uncertainty range. We took into account the RH variations in the DMA. At IZO, the RH of the DMA always stayed below 10%. At PDH, the median RH in the DMA was 6%, the average was 15%. It reached exceptionally values as high as 40%. The sensitivity to the cut-off sharpness was addressed by calculating the aerosol volume assuming a sharp cut, and using the real sampler impaction efficiency. The uncertainty in aerosol volume generated by counting and sizing errors was assessed through sensitivity tests because flow uncertainties have non independent effects on sizing and counting in a DMA. Finally, the dry aerosol mass concentration m_{SD} was calculated as:

$$m_{SD} = d_0 \times V(D_s)/GF_s^3, \quad (9.5)$$

and formula (9.1) was applied to estimate the overall uncertainty of m_{SD}.

Eq. (9.1) was also applied to estimate the random uncertainties in average concentrations of the aerosol components. The overall uncertainty in the average concentration of each aerosol component was calculated by adding conservatively the random uncertainty in the average concentration of this component and the possibly systematic errors associated with the measurement of this component.

REFERENCES

Ananth, G. and Wilson, J. G. 1988. Theoretical analysis of the performance of the TSI aerodynamic particle sizer. The effect of density on response. *Aerosol Sci. Technol.* **9**, 189–199.

Bates, T. S., Calhoun, J. A. and Quinn, P. K. 1992. Variations in the metahnesulfonate to sulfate molar ratio in submicrometer marine aerosl particles over the South Pacific Ocean. *J. Geophys. Res.* **97**, 9859–9865.

Berge, E. 1997. (ed.) *Emissions, dispersion and trends of acidifiying and eutrophying agents.* EMEP/MSC-W Status Report 1997 Part 1, Oslo, Norwey.

Cachier, H. 1998. Carbonaceous combustion aerosol. In: *Atmospheric particles* (eds. R. M. Harrison and R. Van Grieken). IUPAC, Envrironmental Ser., John Wiley & Sons Ltd, New York, pp. 295–348.

Chow, J. C., Watson, J. G., Pritchett, L. C., Pierson, W. R., Frazier, C. A. and Purcell, R. G. 1993. The DRI thermal/optical reflectance carbon analysis system: description, evaluation and applications in the US air quality studies. *Atmos. Environ.* **27A**, 1185–1201.

Eatough, D. J., Wadsworth, A., Eatough, D. A., Crawford, J. W., Hansen, L. D. and Lewis, A. D. 1993. A multiple-system, multi-channel diffusion denuder sampler for the detremination of fine-particulate organic material in the atmosphere. *Atmos. Environ.* **27A**, 1213–1219.

Eatough, D. J., Eatough, D. A., Lewis, L. and Lewis, A. D. 1996. Fine particulate chemical composition and light extinction at Canyonlands National Park using organic particulate material concentrations obtained with a multisystem, multichannel diffusion denuder sampler. *J. Geophys. Res.* **101**, 19515–19531.

Fischer, H., Nikitas, C, Parchatka, U., Zenker, T., Harris, G. W., Matuska, P., Schmitt, R., Mihelcic, D., Muesgen, P., Paetz, H. W., Schultz, M. and Volz-Thomas, A. 1998. Trace gas measurements during the Oxidizing Capacity of the Tropospheric Atmosphere campaign 1993 at Izaña. *J. Geophys. Res.* **103**, 13505–13518.

Fitz, D. R. 1990. Reduction of positive organic artifact on quartz filters. *Aerosol Sci. Technol.* **12**, 142–148.

Gray H. A., Cass, R. G., Huntzicker, J. J., Heyrdahl, E. K. and Rau, J. A. 1986. Characteristics of atmospheric organic and elemental carbon particle concentrations in Los Angeles. *Environ. Sci. Technol.* **20**, 580–589.

Hegg, D. A., Livingston, J., Hobbs, P. V., Novakov, T. and Russel, P. 1997. Chemical apportionment of aerosol column optical depth off the mid-Atlantic coast of the United States. *J. Geophys. Res.* **102**, 25293–25303.

Heintzenberg, J. 1989. Fine particles in the global troposphere, a review. *Tellus* **41B**, 149–160.

Hering S. V. et al. 1990. Comparison of sampling methods for carbonaceous aerosols in ambient air. *Aerosol Sci. Technol.* **12**, 200–213.

Huebert, B. J., Howell, S. J., Zhuang, L., Heath, J. A., Litchy, M. R., Wylie, D. J., Kreidler-Moss, J. L., Cöppicus, S. and Pfeiffer, J. E. 1998. Filter and impactor measurements of anions and cations during the first Aerosol Characterization Experiment (ACE 1), *J. Geophys. Res.* **103**, 16493–16509.

Intergovernmental Panel on Climate Change (IPCC). 1996. *Climate Change 1995*. (eds. J. T. Houghton et al.). Cambridge Univ. Press, New York.

John, W., Hering, S., Reischl, G. and Sasaki, G. 1983. Characteristics of Nuclepore filters with large pore

size-II. Filtration properties. *Atmos. Environ.* **17**, 3037–3038.

Kahl, J. D. 1993. A cautionary note on the use of air mass trajectories in interpreting atmospheric chemistry measurements. *Atmos. Environ.* **27A**, 3037–3038.

Khlystov, A., Wyers G. P. and Slanina, J. 1995. The steam jet aerosol collector. *Atmos. Environ.* **29**, 2229–2234.

Loo, B. W. and Cork, C. P. 1988. Development of a high efficiency virtual impactor. *Aerosol Sci. Technol.***9**, 167–176.

Malm, W. C., Geghart, K. A., Molenar, J., Cahill, T., Eldred, R. and Huffman, D. 1994. Examining the relationship between atmospheric aerosols and light extinction at Mount Rainier and North Cascades national parks. *Atmos. Environ.* **28**, 347–360.

Mangoni. M. and Putaud. J. P. 1998. The sulfur cycle in clean and polluted air masses in the marine boundary layer during ACE-2. *Joint International Symposium on Global atmospheric chemistry*. University of Washington, August 19–25, Seattle, USA.

Neusüß, C., Weise, D., Birmili, W., Wex, H., Wiedensohler, A. and Covert, D. 2000. Size-segregated chemical, gravimetric and number size distribution derived mass closure of the aerosol in Sagres, Portugal, during ACE-2. *Tellus* **52B**, 169–184.

Novakov, T., Hegg, D. A. and Hobbs, P. V. 1997. Airborne measurements of carbonaceous aerosols on the East coast of the United States. *J. Geophys. Res.* **102**, 3023–30030.

Novakov, T., Bates, T. S. and Quinn, P. K. 2000. Shipboard measurements of concentrations and properties of carbonaceous aerosols during ACE-2. *Tellus* **52B**, 228–238.

Quinn, P. K. and Coffman, D. J. 1998. Local closure during the First Aerosol Characterization Experiment (ACE 1): Aerosol mass concentration and scattering and backscattering coefficients. *J. Geophys. Res.* **100**, 2893–2903.

Quinn, P. K., Bates, T. S., Coffman, D. J., Miller, T. L., Johnson, J. E. and Covert, D. S. 2000. A comparison of aerosol chemical and optical properties from the first and second aerosol characterization experiments. *Tellus* **52B**, 239–257.

Raes, F. 1995. Entraiment of free tropospheric aerosols as a regualting mechasnism for cloud condensation nuclei in the remote boundary layer. *J. Geophys. Res.* **103**, 16575–16596.

Raes, F., Van Dingenen, R., Cuevas, E., Van Velthoven, P. F.J. and Prospero, J. M. 1997. Observations of aerosols in the free troposphere and the marine boundary layer of the subtropical Northeast Atlantic: Discussion of the preocesses determining their size distribution. *J. Geophys. Res.* **102**, 21315–21328.

Schwikowski, M. Seibert, P., Baltensberger, U. and Gäggeler, H. W. 1995. A study of an outstanding Saharan dust event at the high-alpine site Jungfraujoch, Switzerland. *Atmos. Environ.* **29**, 1829–1842.

Swietlicki, E., Zhou, J., Covert, D. S., Hämeri, K., Busch, B., Vakeva, M., Dusek, U., Berg, O. H., Wiedensohler, A., Aalto, P., Mäkelä, J., Marinsson, B. G., Papaspirodopoulos, G., Mentes, B., Frank, G. and Stratmann, F. 2000. Hygroscopic properties of aerosol particles in the north-eastern Atantic during ACE-2. *Tellus* **52B**, 201–227.

Van Dingenen, R., Raes, F., Putaud, J. P., Virkkula, A., Mangoni, M. 1999. Processes determining the relationship between aerosol number and non-sea-salt sulfate mass concentrations in the clean and perturbed marine boundary layer. *J. Geophys. Res.* **104**, 8027–8038.

Van Dingenen, R., Virkkula, A. O., Raes, F., Bates, T. S. and Wiedensohler, A. 2000. A simple non-linear relatioship between submicron aerosol number and volume, explaining their observed ratio in the clean and polluted marine boundary layer. *Tellus* **52B**, 239–251.

Verver, G., Raes, F., Vogelzang, D. and Johnson, D. 2000. The second Aerosol Characterization Experiment (ACE-2): meteorological and chemical context. *Tellus* **52B**, 126–140.

Wolff, G. T., Ruthkosky, M. S., Stroup, D. P. and Korsog, P. E. 1991. A characterization of the principal PM-10 species in Claremont (summer) and long beach (fall) during SCAQS. *Atmos. Environ.* **25A**, 2173–2186.